AN EXPERIMENTAL STUDY ON BOUNDARY LAYER SEPARATION CONTROL OVER S809 AIRFOIL USING SYNTHETIC JET ACTUATORS

A THESIS SUBMITTED TO
THE GRADUATE SCHOOL OF NATURAL AND APPLIED SCIENCES
OF
MIDDLE EAST TECHNICAL UNIVERSITY

BY

MELİKA GÜL

IN PARTIAL FULFILLMENT OF THE REQUIREMENTS
FOR
THE DEGREE OF MASTER OF SCIENCE
IN
AEROSPACE ENGINEERING

SEPTEMBER 2013

Approval of the thesis:

AN EXPERIMENTAL STUDY ON BOUNDARY LAYER SEPARATION CONTROL OVER S809 AIRFOIL USING SYNTHATIC JET ACTUATORS

submitted by **MELİKA GÜL**in partial fulfillment of the requirements for the degree of **Master of Science in Aerospace Engineering Department, Middle East Technical University** by,

Prof. Dr. Canan ÖZGEN ______________________
Dean, Graduate School of **Natural and Applied Sciences**

Prof. Dr. Ozan TEKİNALP ______________________
Head of Department, **Aerospace Engineering**

Prof. Dr. İ. Sinan AKMANDOR ______________________
Supervisor, **Aerospace Engineering Dept., METU**

Assoc. Prof. Dr. Oğuz UZOL ______________________
Co-Supervisor, **Aerospace Engineering Dept., METU**

Examining Committee Members:

Prof. Dr.M. Cevdet ÇELENLİGİL ______________________
Aerospace Engineering Dept., METU

Prof. Dr. İ. Sinan AKMANDOR ______________________
Aerospace Engineering Dept., METU

Assoc. Prof. Dr.Oğuz UZOL ______________________
Aerospace Engineering Dept., METU

Assist. Prof. Dr. Ali Türker KUTAY ______________________
Aerospace Engineering Dept., METU

Assist. Prof. Dr.Kıvanç AZGIN ______________________
Mechanical Engineering Dept., METU

Date: 04.09.2013

I hereby declare that all information in this document has been obtained and presented in accordance with academic rules and ethical conduct. I also declare that, as required by these rules and conduct, I have fully cited and referenced all material and results that are not original to this work.

Name, Last Name :Melika Gül

Signature :

ABSTRACT

AN EXPERIMENTAL STUDY ON BOUNDARY LAYER SEPARATION CONTROL OVER S809 AIRFOIL USING SYNTHETIC JET ACTUATORS

Gül, Melika
M.Sc., Department of Aerospace Engineering
Supervisor : Prof. Dr. İ. Sinan Akmandor
Co-Supervisor: Assoc. Prof. Dr. Oğuz Uzol

September 2013, 58 Pages

This thesis presents the results of an experimental study that investigates the effect of periodic excitation from individually controlled synthetic jet actuators on the separated shear layer and wake of a model wing that has S809 airfoil profile. The synthetic jet array consists of three individually controlled synthetic jet actuators driven by piezoelectric diaphragms located at 28% chord location near the middle of the span of the blade. In the first part of the study, hot wire and surface pressure measurements are conducted without synthetic jet actuators as a baseline case at Reynolds numbers, namely $2.3x10^5$, $3.4x10^5$ and $5.1x10^5$, at zero angle of attack. The objective is to resolve the size and characteristics of separated shear layer and wake. Afterwards, the effect of the synthetic jet actuators on the separated shear layer and wake is investigated at $2.3x10^5$ Reynolds number at zero angle of attack. Results show that periodic excitation from the synthetic jet actuators is effective in eliminating laminar separation bubble. In addition, this study provides information about flow physics related to the interaction between the synthetic jet flow and the adverse pressure gradient laminar boundary layer.

Keywords: Active Flow Control, Synthetic Jet Actuators, Boundary Layer Separation Control, Wind Turbine Load Control

ÖZ

SENTETİK JET KULLANARAK S809 KANAT KESİTİ ÜZERİNDE SINIR TABAKASI AYRILMASI KONTROLÜNÜN DENEYSEL İNCELENMESİ

Gül, Melika
Yüksek Lisans, Havacılık ve Uzay Mühendisliği Bölümü
Tez Yöneticisi : Prof. Dr. İ. Sinan Akmandor
Ortak Tez Yöneticisi : Doç. Dr. Oğuz Uzol

Eylül 2013, 58 sayfa

Bu çalışma, bireysel kontrol edilen sentetik jet mekanizmasının ürettiği periyodic salınımların S809 kanat kesidi üzerinde sınır tabaka ayrılmasına ve kuyruk arkasında kalan kısıma etkisini deneysel olarak incelenmesinin sonuçlarını sunmaktadır.Piezoelektrik diyaframlar ile çalıştırılan, bireysel olarak kontrol edilen ve toplam 3 adet olan sentetik jet dizisi kanadın ortasına ve kanat genişliğinin %28'ine konumludur. Çalışmanın ilk kısmında sıfır hücum açısında ve $2.3x10^5$,$3.4x10^5$ ile $5.1x10^5$ Reynolds sayılarında referans değerleri için hot wire ve yüzey basınç ölçümleri yapılır. Bundaki amaç sınır tabaka ayrımının ve kanadın kuruk arkasında kalan akışın büyüklüğünü ve özelliklerini belirlemektir. Daha sonra, sıfır hücum açısında ve $2.3x10^5$Reynolds sayısında, sentetik jetin sınır tabakası ayrılması üzerine ve kanadın kuruk arkasında kalan akışa olan etkisi incelenir. Sonuçlar sentetik jetlerin laminar akım boncuğunun yok edilmesinde etkili olduğunu göstermektedir. Ek olarak, bu çalışma sentetik jetlerin ters basıç gradyanı altındaki sınır tabaka ile olan etkileşimi hakkında da bilgi sunmaktadır.

Anahtar Kelimeler: Aktif Akış Kontrolü, Sentetic Jet Aktüatörler, Sınır Tabaka Ayrılması Kontrolü, Rüzgar Türbini Yük Kontrolü.

To my family

ACKNOWLEDGMENTS

I would like to express my gratitude to my supervisor Dr. İ. Sinan Akmandor. Although he did not give me the traditional supervision expected by a graduate student, he encouraged me to grow into an independent researcher. I am sure this was a great experience for me. Also, I would like to thank my co-supervisor Dr. Oğuz Uzol for his support during my graduate studies. I am grateful to my colleagues and friends Ezgi Anık, Merve Tıraş, Gülgün Afacan, Sohaib Tariq Mian, Derya Kaya, Anas Abdulrahim, Nihan Şatgeldi and Mustafa Şahin for their invaluable help during the long and exhausting experiment days.

I would like to thank METU Wind Center for their financial support for manufacturing my blade parts and ordering piezoelectric actuators. This experimental study could not be achieved without the support of METU Wind Center. I appreciate their investment in research. Also, I would like to thank TUBITAK for their scholarship which helped me to pursue my master study.

And.. I would like to express my deepest gratitude and sincere thanks to my dear parents, Güllü and Ali, my sisters Derya and Dilek and my aunt Sevgül Rojda for their endless love, patience and support throughout my life.

TABLE OF CONTENTS

LIST OF TABLES

LIST OF FIGURES

FIGURES

NOMENCLATURE

C_p	Pressure coefficient, $c_p = \dfrac{P_s - P_{s0}}{1/2\rho \bar{U}_0^{\,2}}$
U_0	Free stream mean velocity
C_x	Axial chord [mm]
Re	Reynolds number based on airfoil chord
P_s	Measured local static pressure
P_{s0}	Free stream static pressure
SJA	Synthetic Jet Actuator
d	Width of the slot of the Synthetic Jet Actuator
w	Length of the slot of the Synthetic Jet Actuator
Re_L	Reynolds number based on stroke length (for SJA)
Re_{U0}	Reynolds number based on jet velocity (for SJA)
Re_{I0}	Reynolds number based impulse (for SJA)
L	Stroke length
L_0	Nondimensional stroke length
S	Stokes number
St	Strouhal number
f	Frequency
VR	Jet-to-free stream velocity ratio
$Vp\text{-}p$	Peak-to-peak voltage
c_f	Non-dimensional shear stress
U_e	Local mean edge velocity [m/s]
V_j	Instantaneous jet velocity [m/s]
U	Local mean velocity [m/s]
ρ	Inlet flow density [kg/m^3]
u'	Fluctuating velocity [m/s] $u' = \sqrt{\dfrac{\left(\sum_{i=1}^{N}(U_i - \bar{U})^2\right)}{N}}$
U_i	Instantaneous velocity [m/s]
PIV	Particle Image Velocimetry
$-\overline{uv}$	Reynolds shear stress per unit mass [m^2/s^2]

CHAPTER 1

INTRODUCTION

With the rapid growth in wind energy market, turbine rotor size has increased over years. However, with the increase in the rotor size, conventional wind turbine control methods became ineffective for handling turbine rotor loads. The ability of controlling loads on wind turbine rotor blades is a very important issue because controlling loads on wind turbines will result in not only a higher rotor performance but also a decrease in fatigue loads, thus, a decrease in general cost[1].

Another challenging issue for wind turbines is the ability to capture energy at a wide range of wind speeds and flow conditions. Turbine blades do not operate when the wind speed is below the cut in speed of wind turbines. This not only disables harvesting energy at low speeds but also limits wind turbine installation at sites that have low average wind speeds. In order to handle this problem, aerodynamic performance of turbine rotor blades can be improved with appropriate active flow control devices so that energy harvesting from turbine blades at low wind speeds can be possible.

1.1 Literature Survey

1.1.1 Wind Turbine Control

The aim of wind turbine control is to regulate torque and power output, reduce fatigue loads and optimize energy production of wind turbines. There are several types of wind turbine control methods which can be grouped as passive and active control. Active control methods require external energy or auxiliary power whereas passive methods do not require any external energy or auxiliary power. Some passive control methods for wind turbine applications are stall control, yaw (downwind) control, aeroelastic blade twist and passive flow control devices such as mechanical vortex generators and gurney flaps. Active wind turbine control methods include collective pitch control with variable rotor speed, advanced pitch control with cyclic or individual pitch, variable diameter rotor, trailing edge flaps, microtab, microflap, active vortex generators, suction and blowing, plasma and synthetic jet actuators. Some of these control techniques are well known and used for wind turbine applications; on the other hand, most of these control devices have not been matured enough to be tested on wind turbines.

The first commercial wind turbines are stall regulated. With stall regulation control, the blade pitch is fixed and the turbine rotational speed is near constant. When the wind speed increases the angle of attack of the blades also increases. With further increases in the wind speed the blades finally stall which decreases lift and increases drag. Although stall control of wind turbine blades is very simple, this method is uneconomical for large rotor blades [2]. With the increase in rotor sizes, collective pitch control with variable speed rotors has been developed. This is an active control method and today most of the large wind turbines utilize this control. Pitching causes the blades to rotate around its spanwise axis in order to alter the inflow angle as a response to the changes in the wind. Variable speed rotors and collective pitch method is more effective than stall regulation control; however, this method is slow to respond changes in the wind conditions for large wind turbines and is not capable of handling the loads caused by rotor yaw errors, wind shear, wind gusts, shaft tilt, wind upflow and turbulence[3].

In order to tackle with ultimate and fatigue loads new advanced control methods are being investigated. One of these advanced control method is called advanced pitch control which includes cyclic and individual pitch control concepts. Cyclic pitch method, initially known from helicopter control, changes the blade pitch angles with a phase difference of 120 degrees in order to reduce the variations in the rotor tilt and yaw moment, and individual pitch control adjusts the individual blade pitch instantaneously based on the local flow data [4]. These advanced pitch control methods are applied together with collective pitch control. Individual pitch control studies of Bossanyi et al.showed a decrease in fatigue loads of 30-40% at the hub and 20-30% at the blade roots [5]. Similarly, Larsen et al. found fatigue load reduction on the order of 9-31% on several wind turbine components with individual pitch control [4]. In addition, since advanced pitch control methods require local wind data such as local inflow angle and flow velocity, new approaches were developed by Van der Hooft and Van Engelen [6]and Hand et al. [7]. Van der Hooft and Van Engelenproposed the estimation of incoming wind speed using energy balance, and Hand et al.used a LIDAR (Light Detection and Ranging) system to directly measure the local flow data. However, despite its proved effectiveness on load reduction, individual pitch control suffer some problems[8].First, large rotor sizes, for multi-MW blades, can limit the response of the pitch actuator; therefore, sufficient load reduction may not be achieved. He proposed to tackle with this problem by using control devices based on real time measured quantities along the blade span. Second, excessive use of pitch control may damage the pitch bearings and actuators. Third, high pitch angles and rates are needed especially when controlling the fluctuating loads due to turbulence.

Another wind turbine control method is variable rotor diameter which has been developed to improve the energy capture at low speed and reduce the loads on the blades at high speeds through extending and retracting the blade tip respectively. DOE with the collaboration of Energy Unlimited, and Knight and Carver manufactured and tested variable turbine blades with variable rotor diameter which can change from 8m to 12 m[9].According to the field tests of the prototype, they stated that output power can be raised by 20-50% above the power that a standard blade with 9 meter can achieve when the wind speed changes from 7 m/s to 9m/s. In addition, according to the report published by GE Wind Energy [10]a full size turbine with variable rotor size can decrease the COE by 18%. However, this control type includes some challenging issues such as complex control strategies, high aerodynamic efficiency, increased blade weight, and durability and reliability of the system [11].

In order to regulate the power and control wind turbine rotor aerodynamics with aileron type devices, several wind tunnel experiments, numerical simulations and field tests were conducted by the National Renewable Energy Laboratory (NREL) during the 90s. These studies form the first studies that aerodynamic control devices on wind turbine blades have been investigated. Since these trailing edge flaps are heavy, slow and very big, non conventional trailing edge flap concept has been introduced with piezoelectrics and smart materials system [11].The Adaptive Trailing Edge Geometry (35-39) is a kind of deformable trailing edge flap made of piezoelectric actuators. Bak et al. [12]carried out wind tunnel tests on Risoe B1-18 airfoil with a 9%c flap made of TH-6R piezoelectric bender actuators. Tests were carried out at Re=1.66x10^6 and they found that a step change of the ATEG from -3(deflection towards the suction side) to +1.8 (deflection towards the pressure side) can generate a change in lift from 0.10 to 0.13 in the linear lift region. Their experiments also showed that the ATEG is capable of decreasing the load variations in sinusoidal pitch motion. Hulskamp et al. at Delft University Wind Energy Research Institute, performed wind tunnel experiments on a reduced scale wind turbine blade and with feedback control they achieved a reduction in root strains from 60% to 95%[13]. Although these nonconventional trailing edge flaps seem promising, as stated by Johnston et al. [11], they have several drawbacks and require additional research regarding the issues such as scalability to large models, the durability and reliability of the deployment structures and the power to actuate the control surfaces.

Boundary layer control techniques forms another group that is recently being researched to control the loads on wind turbine blades. Suction, blowing, active vortex generators, synthetic jets and plasma actuators are some examples of boundary layer control methods. Suction is the principle to remove low momentum fluid near the surface and therefore diverting high momentum fluid towards the surface, and blowing is the method to add momentum to the decelerated flow near the surface which affects the boundary layer and prevents separation [14]. Although these two principals have been found to be effective methods for increasing lift and decreasing drag for aircraft applications, as stated by Johnston et al. [11], there are some concerns about the applications of these methods on wind turbine blades. These concerns are additional weight, complexity of spanwise slots and requirement to store the compressed air. Vortex generators are small vanes located on the surface of airfoils. Through the vortices generated by the vanes, the boundary layer of the airfoil gets more energetic and boundary layer separation can be mitigated as a result. However, passive vortex generators cannot adapt to the changes in the flow, therefore, they increase drag. Passive vortex generators have been studied for controlling flow separation near the root region of wind turbine blades [11]. On the other hand, active vortex generators have the ability to adapt to the changes in the flow, and this control method has been proposed by Barrett and Farokhi [15]for active flow control on wind turbine blades. They conducted experiments using ramp-type vortex generators with shape memory alloy actuators (SMA), a shear flow separation sensor and a controller on a NACA airfoil at Re=$4.27 \times 10^4$and found that active VGs have the ability to delay stall. Surface non-thermal plasma actuators utilize discharged-induced electric wind caused by the voltage difference applied between two or more electrodes in order to control the flow characteristics within the boundary layer [16]. Although there are several types of plasma actuators, surface dielectric barrier discharge (DBD) plasma actuators are widely used for flow control on airfoils due to its simple use that makes researchers in aerodynamics to study these control type without being an expert on plasma physics [16]. A review of DBD plasma actuator studies demonstrating the effectiveness of these actuators on flow control over airfoils can be found in the study conducted by Corke et al.[17]. In order to investigate the feasibility of DBD plasma actuators on lift control over wind turbine airfoils, Nelson et al.[18]conducted experiments on S827 and S822 airfoils using surface DBD plasma actuators. With DBD plasma actuators, they modified the effective camber by circulation, and increased the maximum lift coefficient by leading-edge separation over S827 airfoil. With a single steady plasma actuator located at 0.78c, they achieved a 0.008 increase in lift coefficient which is equal to the effect that a 2 degrees of deflection of a plane flap with Cf/C=0.1 can create. Also, they modified the S822 airfoil profile to generate separation ramps that can be controlled by plasma actuators; therefore, they can control the overall lift by modifying the pressure distribution near the trailing edge. With plasma actuators, they recovered the lost in the lift that was caused by separation over the ramps at low angles of attack between $-3<\alpha<3$. Between these angles, the maximum lift change is about 0.4 with plasma actuators on and off conditions, which is equal to the change that a 10 degrees deflection of a plane trailing edge flap can create. Although it has been proven that plasma actuator is an effective way of flow control, there are some issues to be improved such as low efficiency, maintaining a stable plasma region and reduced performance at high speeds [11]. Synthetic jet actuator is another boundary layer control method that is recently being investigated both for aircraft and wind turbine applications. Recently, Stalnov et al. [19]and Maldonado et al. [20]studied the effectiveness of synthetic jet actuators on the airfoil performance. Stalnov et al. performed experimental studies using synthetic jet actuators over a two dimensional IAI pr8-SE airfoil, a thick airfoil suitable for wind turbine rotor blades. They investigated the effect of the actuators on the performance of the airfoil by controlling the boundary layer separation and they compared the results with the ones they obtained using mechanical vortex generators (VG). Based on their experiments, they demonstrated synthetic jet actıators are effective for a wide range of Reynolds number while VGs perform well only at design Reynolds number. In addition, they stated that since synthetic jet actuators are effective in low Reynolds numbers, they can be used to reduce the cut-in speed of wind turbines which as a result will increase the maximum lift of the airfoil at low Reynolds numbers. Maldonado et al. conducted experiments using an array of synthetic jet actuators over a small scale S809 finite wind turbine blade. They investigated the effect of the actuators on the blade's structural vibration by controlling the boundary layer separation at a range of Reynolds number between $7.1 \times 10^4$and 2.38×10^5, and post stall angles of attacks from 15 to 17.5 degrees. They found that there is a relation between the degree of the flow separation and the reduction in the blade's structural vibration.

1.1.3 Synthetic Jet Actuators (SJAs)

A synthetic jet actuator is a device that generates synthesized jet from the ambient fluid through an orifice or slot due to the oscillation of a diaphragm placed on one (or more) of the walls of a sealed cavity. Synthetic jet actuators typically consist of a sealed cavity, an orifice or slot and a diaphragm (an oscillating material) as illustrated in the following picture.

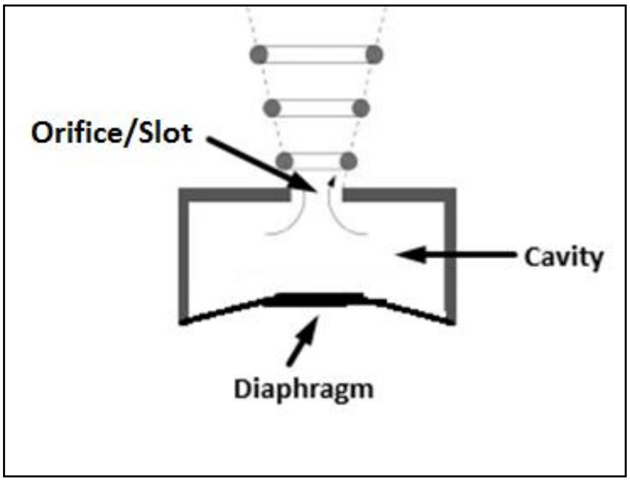

Figure 1.1.1: Schematic of a SJA.

Piezoelectrically driven diaphragms (e.g.[22], [23]) electromagnetically driven pistons (e.g.,[24].) and diaphragms driven by an acoustic source(e.g., [25]) are the common drivers for the diaphragm of a synthetic jet actuator. When the diaphragm of a synthetic jet actuator is excited by one of these methods, the diaphragm deflects and excites the flow inside the cavity. When the diaphragm deflects away from the orifice, the cavity volume increases and the low momentum ambient flow is drawn inside the cavity (suction stroke), and when the diaphragm moves towards the orifice (blowing stroke) this fluid is ejected through the orifice. During the blowing stroke, the ejected fluid separates at the edge of the orifice and if it is sufficiently strong and sufficiently far away from the orifice, it overcomes the suction velocity, therefore, rolls up into vortical structure, and then moves with its self induced velocity. Successive ejection and blowing strokes result in a train of vortex structures moving away from the orifice of the actuator.

A very significant feature of synthetic jets is that they form from the working fluid of the system and therefore they add linear momentum to the system without any mass addition.

That is why they are called zero net mass flux actuators. In addition, due to this zero net mass nature no external plumbing is needed which is one of the advantages of synthetic jet actuators.

In the literature, it is seen that for a given geometry, the formation and the evolution of a synthetic jet under quiscent conditions is described by some nondimensional parameters, namely, non dimensional stroke length (*L*), Reynolds number ($\mathrm{Re}_{U_0}, \mathrm{Re}_L, \mathrm{Re}_{I_0}$), Stokes number (*S*) and Strouhal number (*St*)Non dimensional stroke length (*L*) is defined as the length of the fluid ejected from the orifice/slot of the synthetic jet actuator during the blowing stroke [26].According to Smith and Glezer [22], non-dimensional stroke length and Reynolds number are the primary parameters affecting the behaviour of synthetic jets in quiescent flow. Under crossflow boundary layer, on the other hand, the behaviour of synthetic jet is defined by five independent non-dimensional parameters which are stroke length (*L*), Reynolds number (Re_L), jet-to-free stream velocity ratio (*VR*), the ratio of boundary layer thickness to orifice diameter/ orifice width,(*d*), non-dimensional shear stress (which is equivalent to the skin friction coefficient (c_f)[27].

1.1.3 Low Reynolds Number Airfoil Aerodynamics

When the Reynolds number of the flow is between 10^4-10^6 range, then the flow is defined as low Reynolds number flow. Airfoil performance at low Reynolds numbers is significantly different than its performance at high Reynolds number (e.g.,[28],[29]). At low Reynolds numbers, laminar boundary layer on the upper surface separates due to adverse pressure gradient and a separated shear layer forms as a result. If the separated shear layer reattaches to the airfoil surface, a closed region of recirculating fluid forms within the boundary layer, which is called laminar separation bubble (or transitional separation bubble). Transition from laminar flow to turbulent flow occurs above this bubble. Also, a narrow wake occurs behind the airfoil as a result of this phenomenon. On the other hand, if the flow fails to reattach to the airfoil surface a wide wake forms behind the airfoil. In either case, it is known that laminar boundary layer separation decreases the airfoil performance. Figure 1.1.2 illustrates the time averaged structure of the laminar separation bubble along with the corresponding surface pressure distribution.

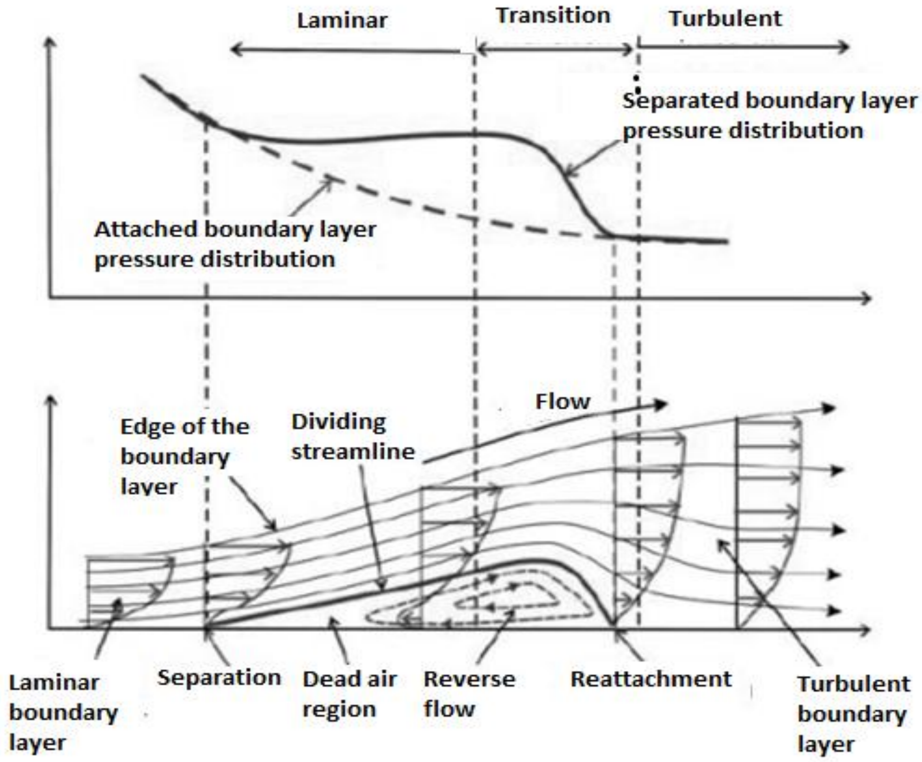

Figure 1.1.2: Time-averaged structure of a two-dimensional separation bubble associated with pressure distribution (Reproduced from Zhang[30]).

As described by Tani[31], the shear layer is stationary in the initial region of the separation bubble which is called dead air region. Following the constant region of stationary fluid, transition begins with a sudden surface pressure recovery and downstream the transition onset reverse flow vortex forms within the separated shear layer [31]. At the aft portion of the separation bubble flow reattaches to the surface, and the reattachment location can be identified with a significant reduction in the rate of surface pressure recovery[32].Separation bubbles formed within the separated shear layer are grouped as short separation bubbles and long separation bubbles. However, it should be noted that apart from their size, separation bubbles are identified by their effects on the surface pressure distribution [33]. If the effect of the bubble on the surface pressure distribution is local, then it is classified as short bubble. On the other hand, if the effect is not local but changes the entire distribution, then the bubble is called as long separation bubble.

1.2 Objectives and Contents of the Study

The preliminary aim of this study is to investigate the effect of synthetic jet actuators on the flow development within the separated shear layer and the wake of the S809 airfoil at a low Reynolds number, $2.3\text{x}10^5$. This study not only examine the potential effectiveness of synthetic jet actuators on flow control at low Reynolds numbers, it also tries to understand the physical process involved. Another aim of the study is to investigate the aerodynamic behaviour ofS809 airfoil at low Reynolds numbers, namely $2.3\text{x}10^5$, $3.4\text{x}10^5$ and $5.1\text{x}10^5$, which are much lower than the designed Reynolds number of this airfoil. This airfoil is chosen for the current study because there is no documented data about this low Reynolds number airfoil at these Reynolds number range.

This thesis consists of four chapters. Chapter 1 introduces the study and presents related literature survey. Chapter 2 includes the experimental setup, procedure and measurement details. Chapter 3 presents and discusses the results obtained from the measurements. Finally, Chapter 4 presents the conclusion, final remarks and future recommendations on the study.

CHAPTER 2

EXPERIMENTAL PROCEDURE

2.1 Experimental Setup

2.1.1 Low-Speed Cascade Wind Tunnel

Experiments are conducted in METUWIND's low speed suction type wind tunnel. This wind tunnel includes a 2D contraction section with an area ratio of 1:5, a fully transparent test section with a cross sectional area of 1x1 m² and a length of 2 m, and it is powered by a 45 kW speed-controlled electrical motor that drives a 1.2 m diameter axial fan. Inlet guide vanes at the entrance of the contraction, a honeycomb and a screen are installed upstream of the test section to maintain appropriate flow quality. Speeds up to about 24 m/s are attainable within the test section.Figure 2.1.1shows a picture of the tunnel.

Figure 2.1.1: Picture of METUWIND's suction type wind tunnel that has a 1 m x 1 m test section area

2.1.2 Wing Model

The wing model used during the experiments has a S809 airfoil profile. The wing span and the chord are 0.99 m and 0.455 m respectively. On the suction side of the wing, a 0.536 m long spanwise part is detachable and there are three different configurations of this detachable part. The first configuration is designed for surface pressure measurements and manufactured from plexiglass with 31 pressure taps located at the mid span in the chordwise direction. The second and third detachable parts are designed for baseline and controlled cases and are made up of ABS plastic. The detachable parts are designed carefully in order to ensure a smooth surface for the boundary layer measurements. Following figure demonstrates pictures of the manufactured wing.

(a)

(b)

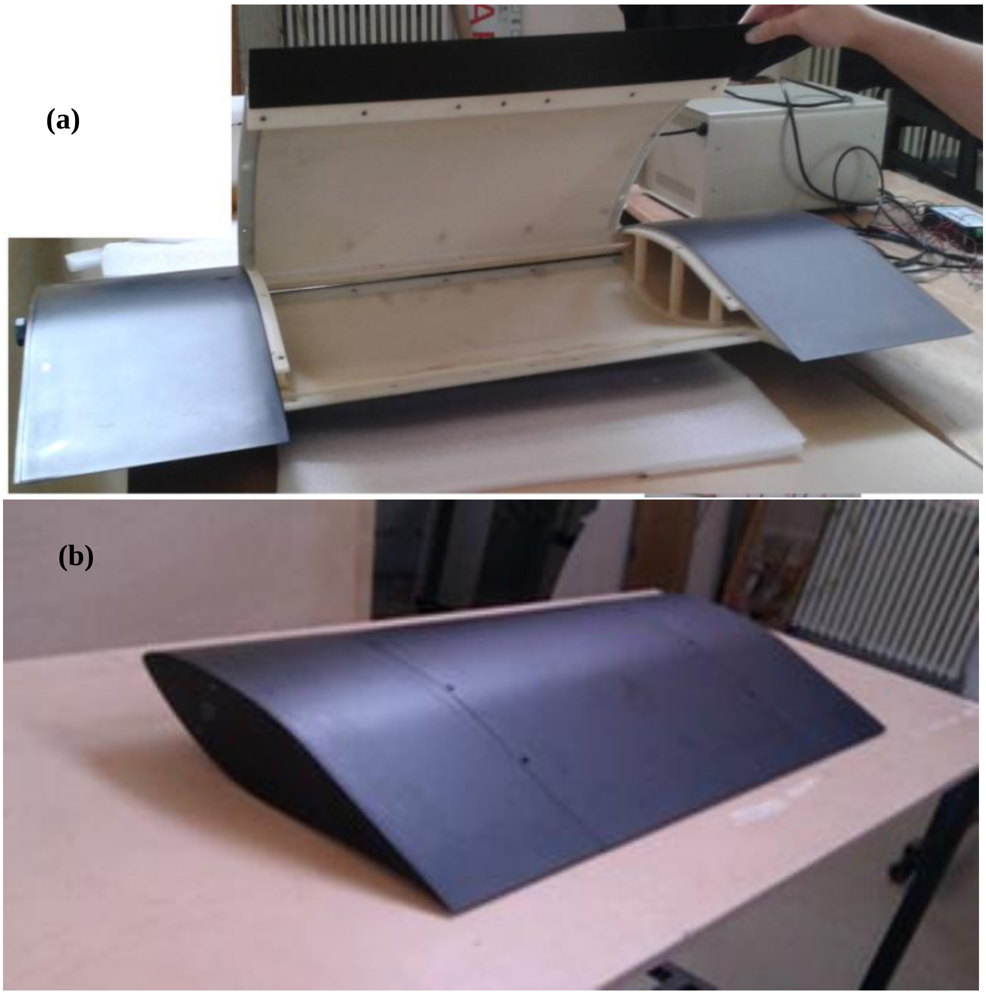

Figure 2.1.2: Manufactured main body integrated with the baseline detachable part (a)exploded (b) compact

The drawings of the parts of the wing modal are demonstrated in the following figure.

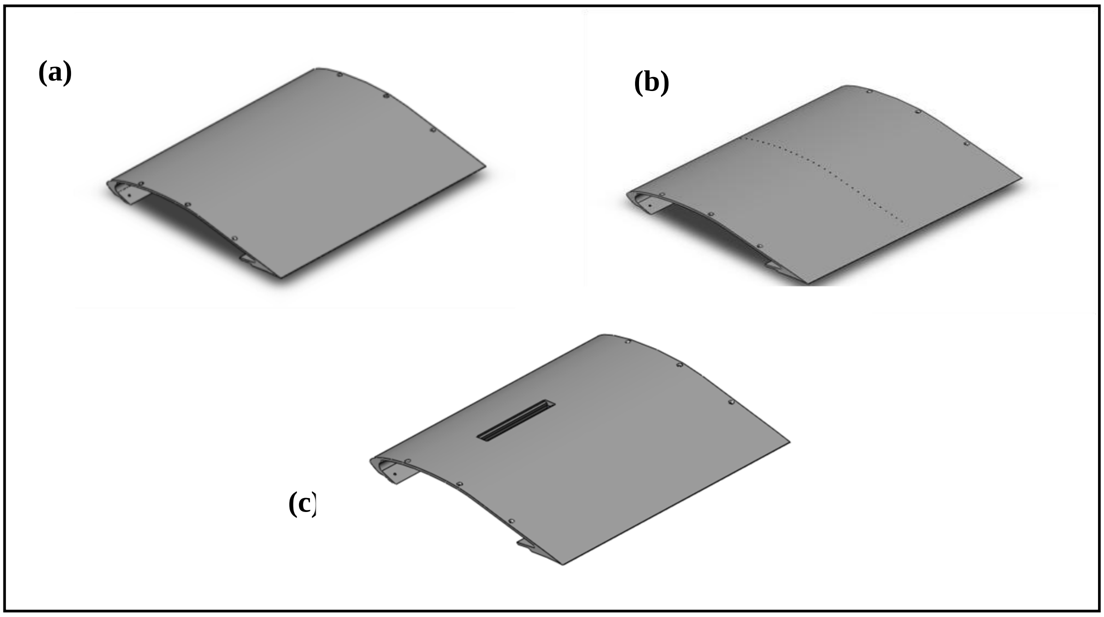

Figure 2.1.3: Detachable upper surfaces (a) for the baseline measurements (b) For the surface pressure measurements (c) for controlled case measurements

The modal blade is put vertically inside the test section with zero angle of attack. The gap between the blade tips and the tunnel walls is 5 mm which is less enough not to affect the results [34].

2.1.3 Synthetic Jet Actuator Configuration

In this study, an array of individually controlled synthetic jet actuatoris designed and manufactured. Each synthetic jet has a rectangular orifice with a width of 0.5 mm, a length of 10 mm and a depth of 1mm, and they are spaced 27.37 mm apart. Thunder 5C piezoelectric actuators manufactured by Face International Cooperation are used to drive the synthetic jet actuators (SJAs).The Thunder 5C actuator, illustrated in Figure 2.1.4is a composite Unimorph ferroelectric Driver and sensor which is composed of three main layers. The first layer is a conductive stainless steel shim with 32.77 mm diameter. The second layer is a PZT with a diameter of 31.75 mm, and the third layer is aluminum with 30.73 mm diameter. These layers are bonded together with a strong adhesive developed by NASA. The total thickness of the Thunder 5C actuator is 0.41 mm.

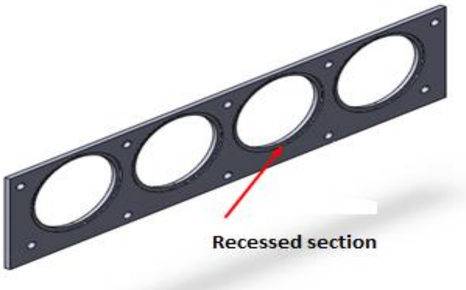

Figure 2.1.4: (a)Thunder 5C[35]   (b)Plexiglass plate with recessed section.

The Thunder 5C actuators can be operated using maximum voltage up to +420V and as low as -210V as long as the total peak to peak voltage does not exceed 420Vp-p. When operated under 420Vp-p Thunder actuator achieve a maximum deflection of 0.17272 mm [35].

The three Thunder actuators are placed in the recessed sections of the plexiglass plate shown in Figure 2.1.4using silicone. Silicone provides an air sealing for the actuator and it keeps the Thunder in the recessed section without limiting its displacement [36].

The array of the synthetic jet actuators is placed at 28% chord location near the middle of the span. Here, it should be noted that the detachable upper part of the blade and the plates for the SJAs are designed for four individually controlled SJAs; however, only three of them are used during the experiments. The slot of the other one that is not utilized is closed.Figure 2.1.5illustrates the exploded and compact view of the SJAs together with their placement on the upper surface, and Figure 2.1.6demonstrates the dimensions of this placement.

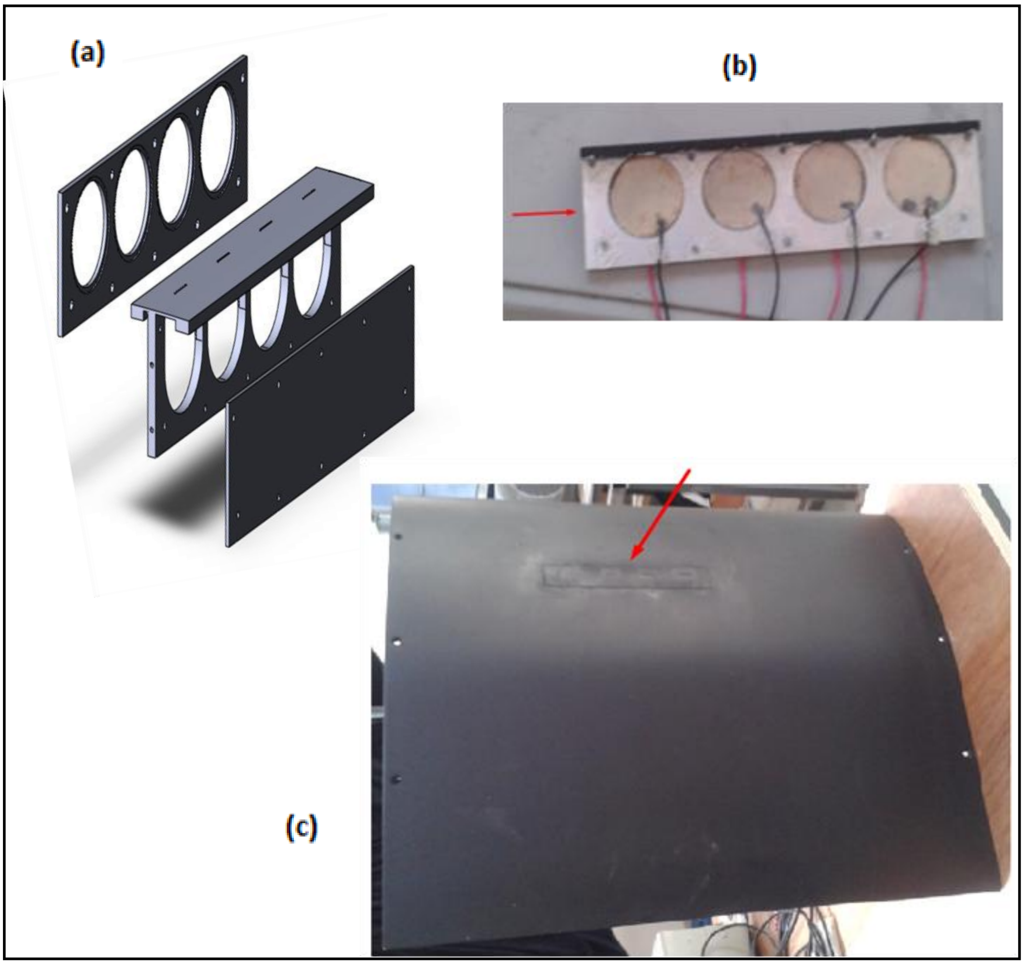

Figure 2.1.5:(a)Exploded and (b)compact view of the SJAs (c) figure showing the place of SJAs on the detachable upper surface of the blade.

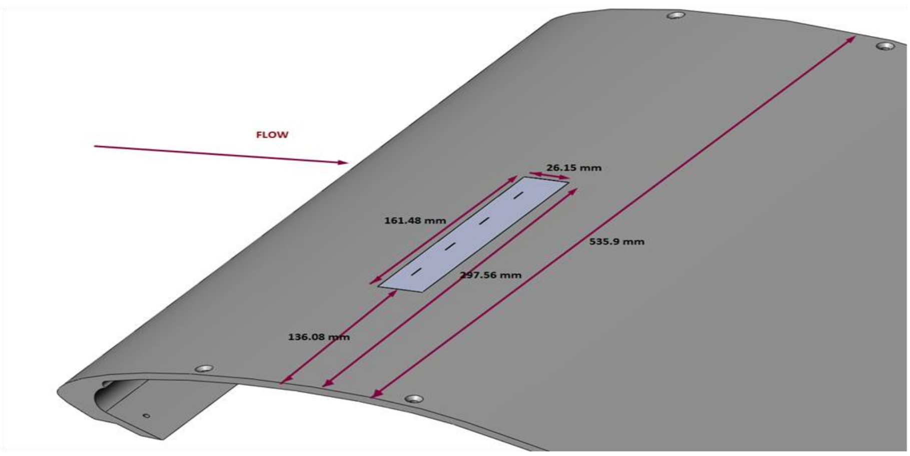

Figure 2.1.6: Drawing showing the position of SJAs on the upper surface of the blade.

2.2 Measurement Details

2.2.1 Surface Pressure Measurements

For the surface pressure measurements, 31 conventional static taps are located at the mid span of the suction surface of the blade in the chordwise direction. The taps are drilled 1 mm in diameter normal to the blade surface with an *l/d* ratio of 2.5. Here,*l* is the length of the drilled hole and *d* is the diameter. With this *l/d* ratio errors in pressure measurements are expected to be independent of this ratio [37]. Also, this *l/d* ratio ensures that the flow within the cavity is fully developed and independent of the Reynolds number [38].

Surface pressure measurements are conducted by a Pressure Systems Incorporated ESP Pressure Scanner. The scanner has 32 channels with 0.03% accuracy. Brass tubes having same inner diameter with the taps are used to connect the taps to Tygon tubings which are connected to the scanner channels. The length of the Tygon tubing is kept as short as possible in order to minimize the errors.

The detachable upper surface with pressure taps can be seen inFigure 2.2.1. Also,

Table **2.2.1**demonstrates the chordwise tap locations.

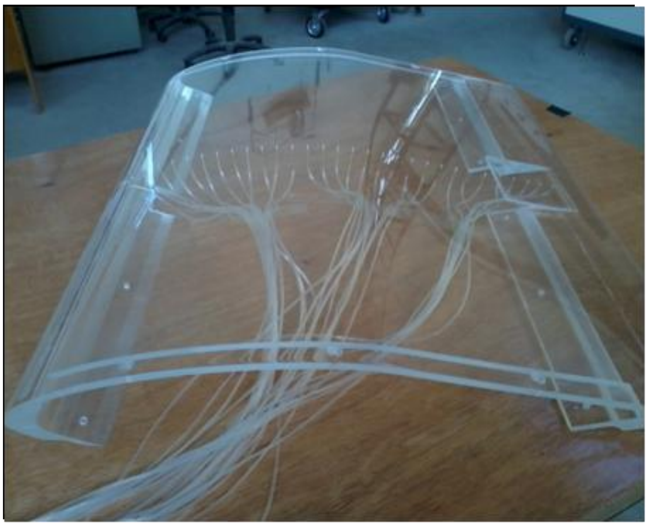

Figure 2.2.1: Upper surface of the blade with pressure taps.

Table 2.2.1: Pressure tap locations

Tap no	**1**	**2**	**3**	**4**	**5**	**6**	**7**	**8**	**9**	**10**
x/c(%)	0	4.12	7.20	10.28	13.36	16.44	19.52	22.6	25.68	28.76
Tap no	**11**	**12**	**13**	**14**	**15**	**16**	**17**	**18**	**19**	**20**
x/c(%)	31.83	34.91	38	41.07	44.15	47.23	50.31	53.39	56.47	59.54
Tap no	**21**	**22**	**23**	**24**	**25**	**26**	**27**	**28**	**29**	**30**
x/c(%)	62.62	65.70	68.78	71.86	74.94	78.02	81.1	84.18	87.26	90.33
Tap no.	**31**									
x/c(%)	93.41									

The static pressure coefficient, C_p, is calculated as:

$$c_p = \frac{P_s - P_{s0}}{1/2\rho \bar{U}^2} \qquad \text{(Eqn. 2.1)}$$

where P_s is the local static pressure on the surface of the airfoil, P_{s0} is the freestream static pressure, $1/2\rho \bar{U}^2$ is the dynamic pressure of the mean flow.

2.2.2 Boundary Layer Measurements Using Hot Wire Anemometry (CTA)

Boundary layer properties are determined using a single wire constant temperature hot wire anemometry. Dantec type 55P11 hot wire probes are used which have a 5μm diameter, platinum plated tungsten wire. The active sensor length is 1.25 mm. Hot-wire probes are calibrated by means of a Dantec54T29 calibration unit. Temperature changes are monitored with a thermometer on the tunnel wall and hot wire is corrected using the Eqn. 2.3.proposed by Bruun [39]for temperature changes up to 2 degrees. The anemometer is connect to a National Instruments digital acquisition board and then to a computer.

$$E_{w,r} = E_w \left(\frac{T_w - T_r}{T_w - T_a} \right)^{(1/2)} \qquad \text{(Eqn. 2.2)}$$

Since the length of the hot wire is 1.25 mm, its output signal is a spaced average signal over this length. Therefore, the instantaneous velocity obtained from the hot wire is the spaced average instantaneous velocity over this wire. Knowing this fact, during the boundary layer measurements at each measurement location, hot wire is positioned parallel to the blade surface so that it measures the spaced averaged instantaneous velocity over a 1.25 mm distance of the span of the blade. That is, the measured instantaneous velocities are the spanwise space averaged velocities. In addition, at each chordwise location, hot wire is traversed along the local boundary layer thickness using VXM stepping motor controller and motorized BiSlides assemblies. The step sizes are remotely controlled with a computer and the accuracy of each step is 0.076 mm. Since the traverse is put outside the tunnel in order not to disturb the flow, chordwise traverse is achieved by manually. Boundary layer measurements are conducted 3.25 cm below the mid span of the blade.

During the characterization of the synthetic jet actuators and controlled case boundary layer measurements, Thunder 5C actuator is driven by a function generator whose output signal is amplified by 15 times using SensortechSA10 High Voltage Power Amplifier. Hot wire and input voltage signals are read at the same time and are processed using Labview.

In addition, during the boundary layer measurements the normal hotwire probe is used to take 10000 instantaneous velocity measurements, while sampling at 5000Hz. During the SJA characterization, on the other hand, 20000 instantaneous velocity data are taken with a sampling rate of 20000 Hz in order to better resolve the mean jet velocity profiles at each actuation frequency which are in the range of 100Hz-2200Hz.

2.2.3 2D Particle Image Velocimetry (PIV) Measurements

A TSI Particle Image Velocimetry (PIV) system, which consists of a30 mJ/pulse Nd:YLF high-speed laser and a 12-bit high-speed Phantom camera,is used for 2D time resolved boundary layer measurements. The high speed camera has the ability to take pictures at 1.5 kHz at a 4 megapixel resolution. A 105mm Macro Sigma lens is used along with a20 mm extension tube in order to increase the magnification. During the experiments, the camera is operated at 742 Hz with 4 megapixel resolution. In fact, this is the maximum resolution attainable when the camera is synchronized with the laser. The camera is traversed between different windows using the Velmex traverse system. The flow is seeded with vaporized olive oil.

During the PIV measurements, the time difference between the two laser pulses (Δt)) is 40 µs which is decided based on pixel displacement between two successive image pairs. Images of four overlapping (35% overlap) windows are taken to resolve the suction surface of the blade after 36.42% chord location. For each measurement window, 285 image pairs are obtained and ensemble-averaged to obtain the average vector field. During the data process, TSI Insight 4G software is utilized in order to obtain the vector maps for each window. An adaptive algorithm starting from 64x64 pixels spot dimensions and decreasing to 32x32 pixels is applied to the raw data with 50% interrogation area overlap along with the post-processing algorithms of vector validation and vector conditioning.

2.2.4 Uncertainty Estimates

Pressure Systems Incorporated ESP Pressure Scanner has an accuracy of 0.03%. However, there arises error also due to tubing. The error caused by temporal changes in the laser pulse synchronization is negligible. The displacement accuracy of the Velmex Traverse System is 0.076mm. For the statistical error arising from the averaging of 285 vector map, it is determined to be less than 8% based on the study conducted by Uzol et al. [44].

CHAPTER3

EXPERIMENTAL RESULTS AND DISCUSSION

3.1 Wind Tunnel Characterization

Performance of low Reynolds number airfoils is highly dependent on the behaviour of laminar boundary layer. Laminar flow behaviour, on the other hand, tends to be affected by high turbulence levels, such that under high turbulence conditions laminar flow attains an early transition to turbulent flow. Therefore, before conducting baseline and controlling case experiments, first, the turbulence intensity of the tunnel are determined for the Reynolds number range that the experiments will be performed.

Turbulence intensity measurements are performed using constant temperature hot wire anemometry that is traversed along the centreline of the inlet of the test section. Since the flow is observed to be highly turbulent at the core region of the tunnel, hot wire is traversed over a 50 cm distance along this centreline with 1 cm grid spacing. Over this distance average and maximum turbulence intensities are determined. Later, same measurements are repeated after the blade is installed in the tunnel, in order to see the effect of the apparatus on the turbulence levels. Measurements are performed over a range of Reynolds numbers with and without the test blade inside the tunnel. Following figures demonstrates the resultant average and maximum turbulence intensities of the suction type wind tunnel at several Reynolds numbers.

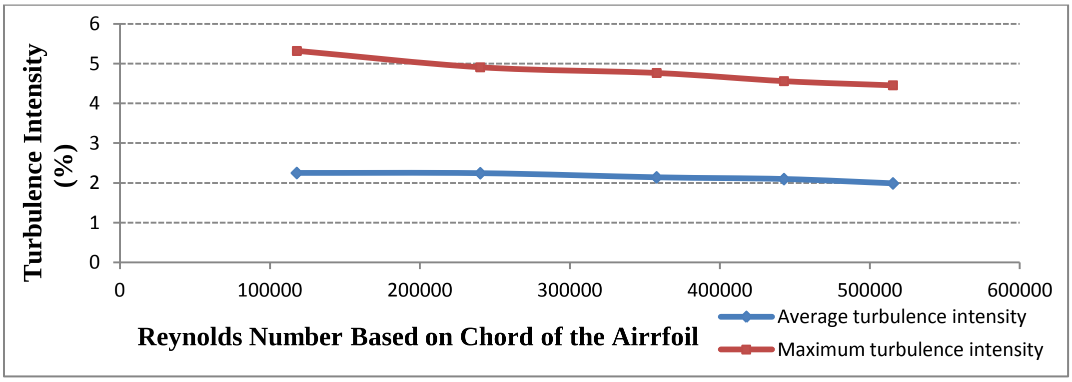

Figure 3.1.1: Average and maximum turbulence intensities along the centreline of the empty tunnel.

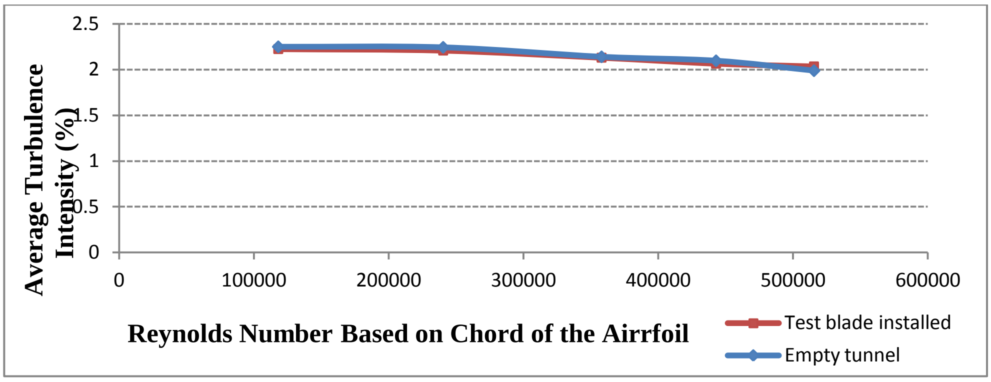

Figure 3.1.2: Comparison of average turbulence intensities of empty tunnel and test blade installed tunnel.

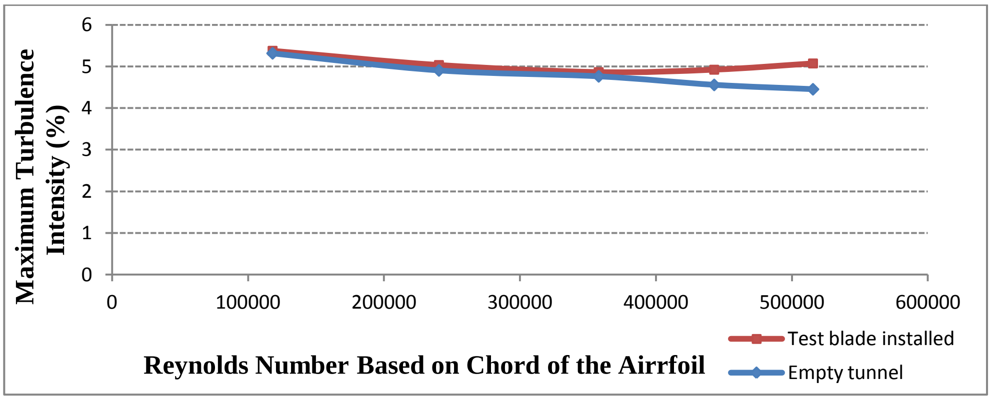

Figure 3.1.3: Comparison of maximum turbulence intensities of empty tunnel and test blade installed tunnel.

For the empty wind tunnel, it is seen from the Figure 3.1.1that both average and maximum turbulence intensities decrease as Reynolds number increases. Therefore, considering the Reynolds number range that the experiments were conducted, average and maximum turbulence intensities are less than 2.25% and 5.32% respectively. For the test blade installed case, from theFigure 3.1.2, it is observed that the average turbulence intensity levels are similar to those in the empty tunnel. That is, the averaged tunnel intensity is not affected much by the test apparatus. Same conclusion can be made for the maximum intensity levels at low Reynolds numbers; however, after a certain Reynolds number maximum turbulence intensity of the blade installed tunnel starts to increase. This may be attributed to the swirling effect of the axial fan of the tunnel. The axial fan is close enough to the test section such that it affects the quality of the flow.

Before closing this part it should be noted that these turbulence intensity levels are quite high; therefore, an early transition from laminar flow to turbulent flow may occur.

3.2 Synthetic Jet Actuator Characterization

During the flow control experiments, the synthetic jet actuators are operated under 300Vp-p. This voltage is decided based on the studies in the literature for synthetic jet actuators driven by Thunder 5C piezoelectric materials. However, for optimization of the actuator further analyses should be conducted in order to determine the optimum operating voltage together with other parameters that effect the behaviour of the synthetic jet under cross flow, such as actuation frequency, Reynolds number, stroke length, boundary layer thickness, skin friction coefficient. In fact, in the literature it is observed that the effect of all these parameters on the synthetic jet behaviour has not been fully understood, therefore, it can be said that studies on synthetic jet actuators are performed, at least mostly, by trial.

Before conducting flow control experiments with the synthetic jet actuators, experiments are conducted under quiescent conditions in order to determine the behaviour of the actuators with no cross flow, and also to decide the operating frequency of the actuator.Figure 3.2.2(a) shows the averaged mean and peak velocities of four realizations at 1 mm above the center of the slot. From the figure it is observed that the maximum mean velocity and maximum peak velocity occur around 2050 Hz. This may be due to the resonant frequency of the Thunder 5C piezoelectric material.

Acoustic frequency of the cavity was determined to be around 1750 Hz based on the formula presented by Gallas [40]. The resonant frequency of the piezoelectric material changes depending on the boundary conditions, and in the figure it is seen that the resonant frequency may occur around around 2050 Hz. This is compatible with the result obtained by Ugrina[36], who mounted the Thunder 5C materials on the cavity using silicone which is a similar boundary condition to the one applied in this study, and found a resultant mechanical frequency of 2200 Hz.

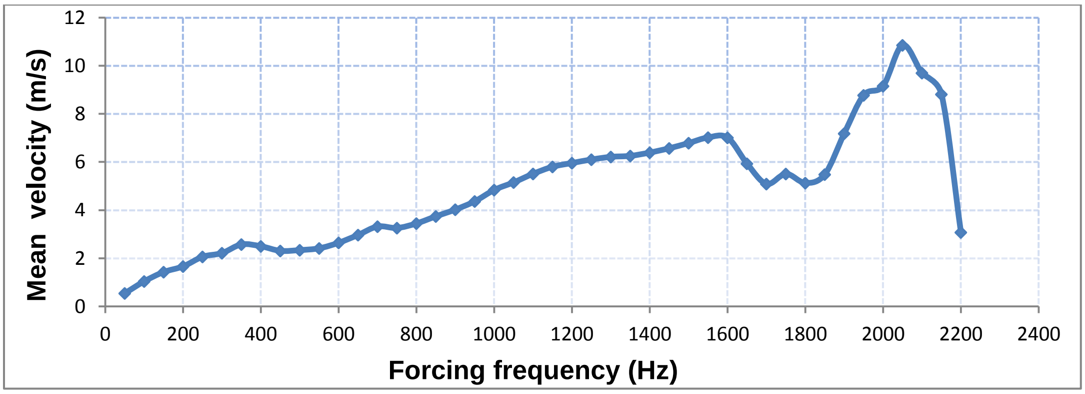

Figure 3.2.1:Average mean jet velocity at 1 mm above the center of the slot at different frequencies

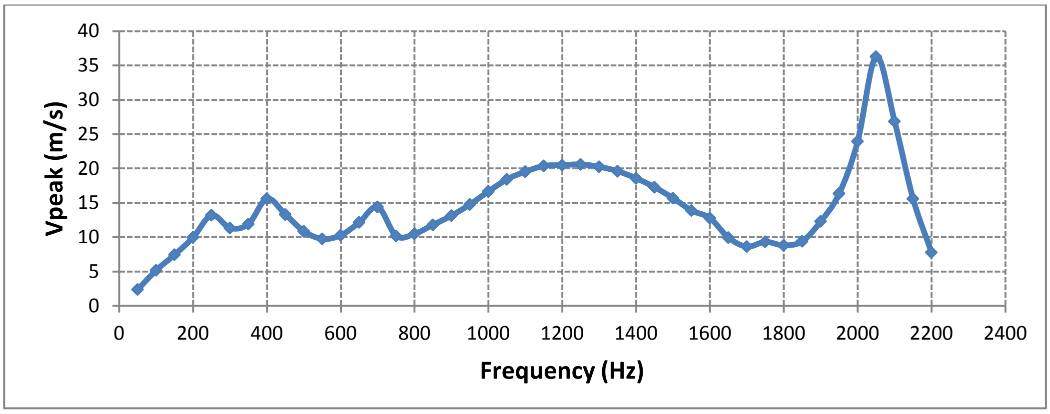

Figure 3.2.2: Average peak jet velocity at 1 mm above the center of the slot at different frequencies

In order to have an insight about the effect of the operating frequency on the structure of synthetic jet, time dependent velocity profiles are determined at several frequencies when driven by a 300Vp-p sinusoidal signal. Some of these profiles are presented in the following figures. Here, Vj represents the instantaneous jet velocity at 1 mm above the center of the actuator slot.

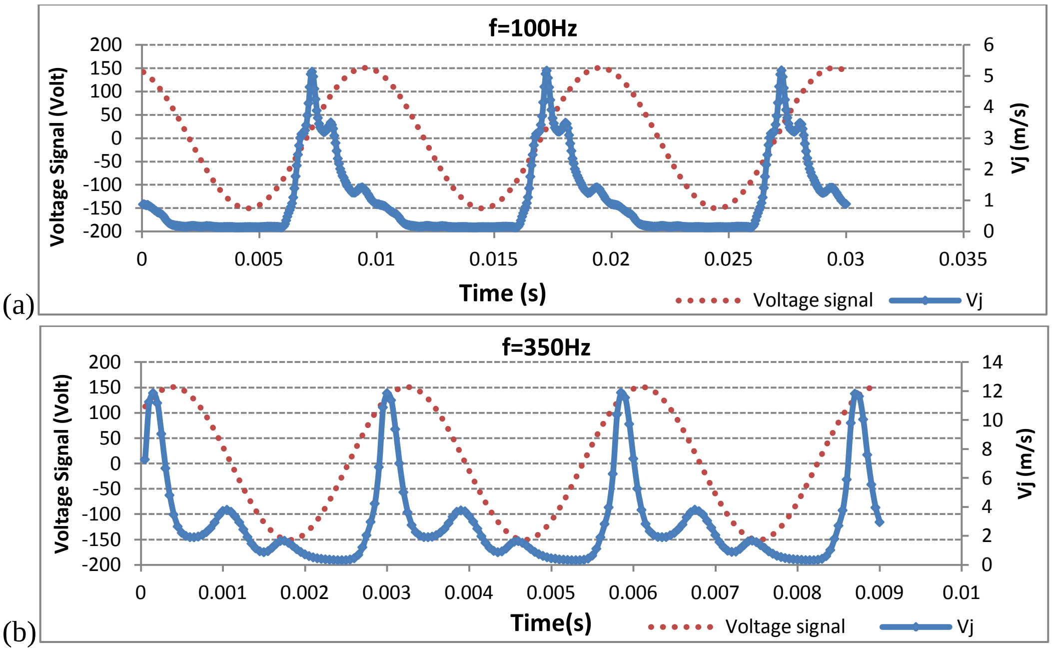

Figure 3.2.3: Time dependent jet exit velocity under (a) 100Hz, (b) 350Hz

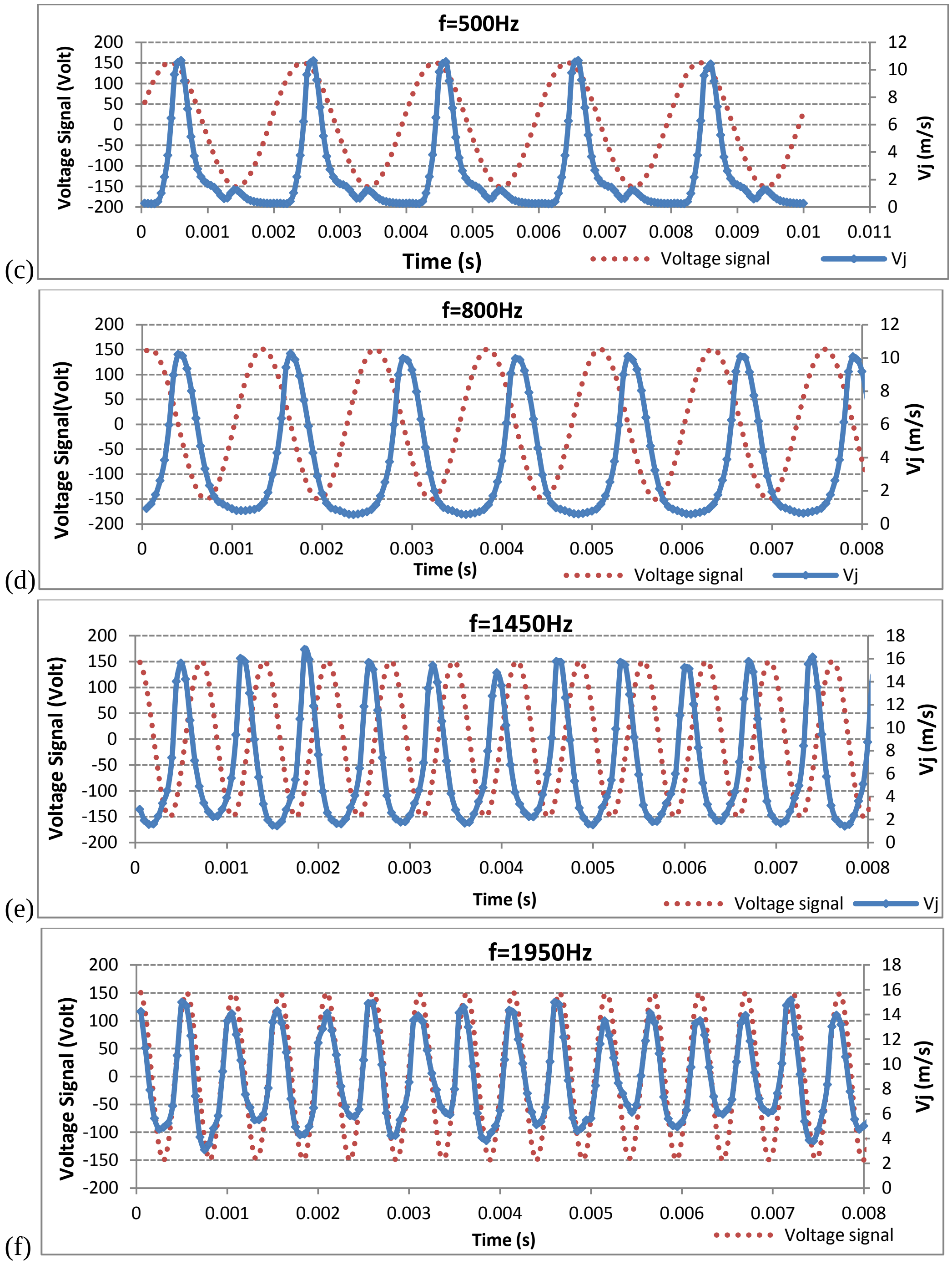

Figure 3.2.4: Time dependent jet exit velocity under (c) 500Hz, (d) 800Hz, (e) 1450Hz, (f)1950Hz

(g) 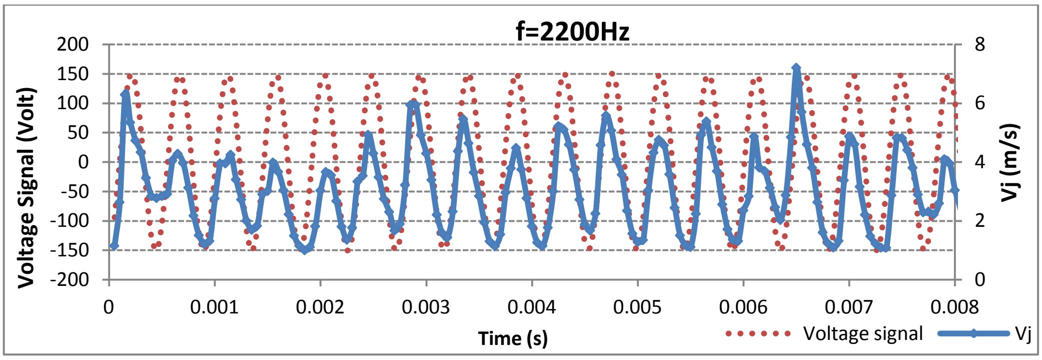

Figure 3.2.5: Time dependent jet exit velocity under (g) 2200Hz

From Figure 3.2.3, Figure 3.2.4and Figure 3.2.5, it is clearly observed that not only the magnitude but also the behaviour of the synthetic jet changes with frequency. It is seen that while zero instantaneous velocities are detected to occur at low frequencies 1 mm above the slot of the actuator, at higher frequencies instantaneous flow velocity does not drop to zero during the cycle. Since the length of the ejected flow during the blowing stroke depends on the frequency at low frequencies the distance that the jet has taken during the blowing stroke may probably not enough for the jet to survive from the suction stroke. That may be the reason of zero instantaneous velocities at low frequencies.

Keeping the above facts in mind, an operating frequency of 1450Hz is decided to drive the synthetic jet actuators since 1450 Hz, which is a moderate frequency generating moderate mean and peak velocities. At the end of the study it will be seen that this frequency is low enough not to trigger the boundary layer separation and high enough to control the flow and eliminate the laminar separation bubble over the airfoil.

After deciding the operating frequency of the synthetic jet actuators, detail velocity measurements are performed at the exit of the synthetic jet actuator along the slot of the actuator.Figure 3.2.6shows the mean jet velocity at 1 mm above the exit of the actuator over a distance from -0.5w to 3.6w, where w is the length of the slot of the actuator. Here, mean jet velocity is normalized by the average center velocity.

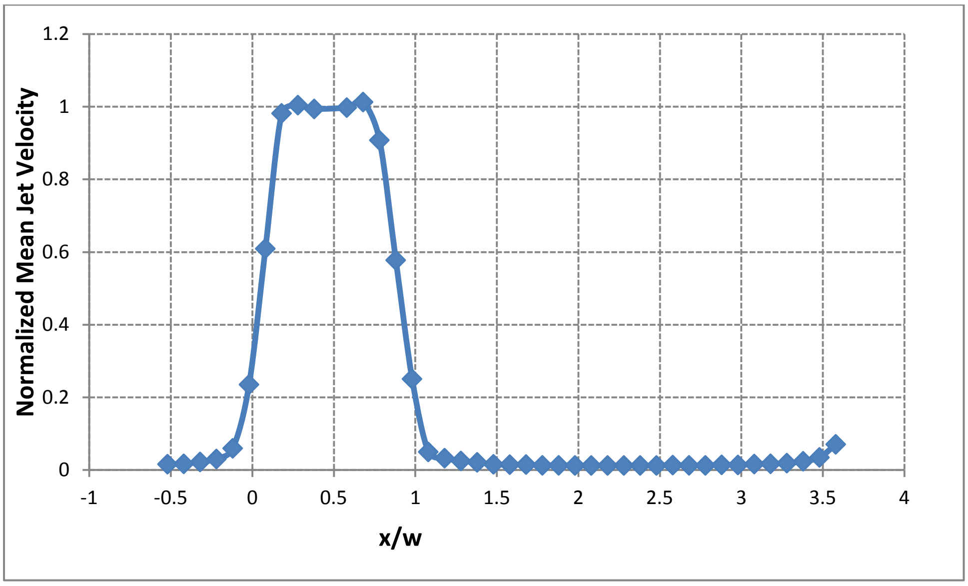

Figure 3.2.6: Mean jet velocity at 1 mm above the exit of the actuator from -0.6w to 3.6w distance.

From the Figure 3.2.6, it is seen that the mean velocity profile along the slot is almost symmetric. Also, after 0.5w downstream the slot, the flow velocity becomes zero and it stays zero for a 1.5w-region between two slots.

3.3 Baseline Measurements (Without Synthetic Jet Actuators)

For the baseline case, flow development within the boundary layer and the wake of the S809 airfoil is studied at three different low Reynolds numbers, namely $2.3x10^5$, $3.4x10^5$ and $5.1x10^5$, at zero angle of attack. The aim is to determine the characteristics of the blade at low Reynolds number. Since the airfoil is observed to have a larger separation bubble on the suction surface of the airfoil at $2.3x10^5$ Reynolds number, this case is studied in detail in this part as the baseline case for the flow control. In the next part, results of the flow control case are presented and the results are compared with the baseline case in order to examine their effect on the flow development within the boundary layer and the wake of the airfoil.

3.3.1 Surface Pressure Measurements

Mid-span surface pressure measurements were performed over the suction surface of theS809 blade at $2.3x10^5$, $3.4x10^5$ and $5.1x10^5$ Reynolds numbers at zero angle of attack. The results are compared with the boundary layer measurements later in the chapter. The details of surface pressure measurements can be found in Chapter 2.

Figure 3.3.1demonstrates time-averaged C_p distributions at $2.3x10^5$, $3.4x10^5$ and $5.1x10^5$ Reynolds numbers at zero angle of attack.

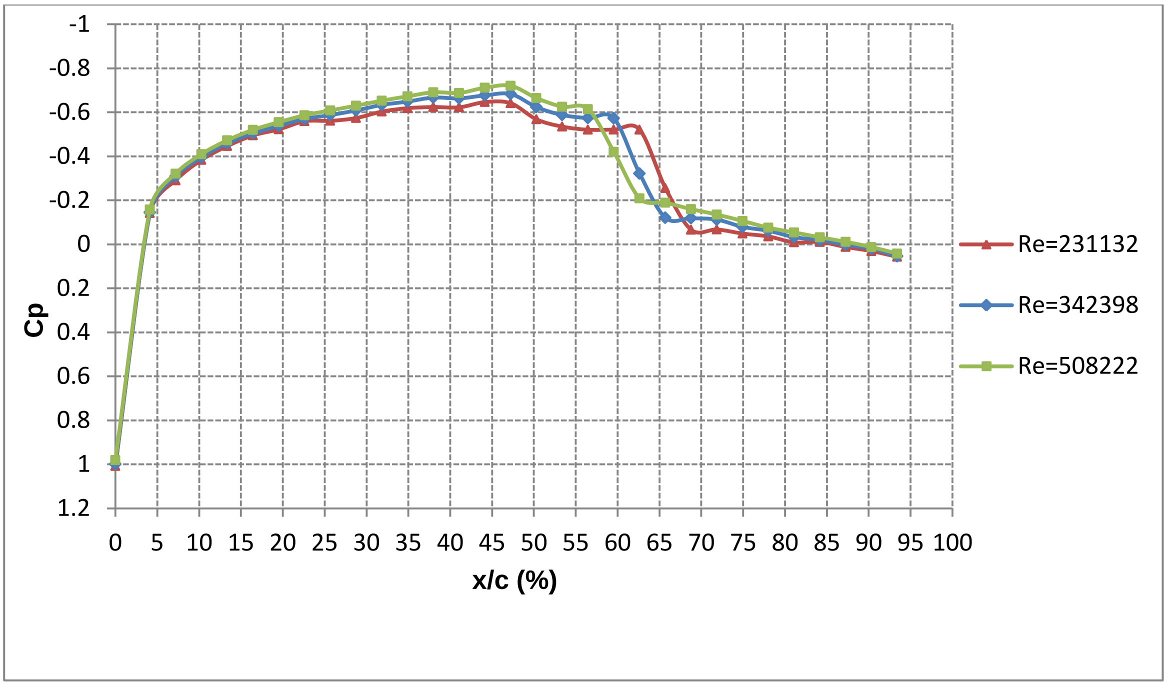

Figure 3.3.1: Surface C_p distribution.

In theFigure 3.3.1, it is clearly seen that for all these low Reynolds numbers, peak suction occurs somewhere between 45% and 50% of chord. For all these three Reynolds numbers boundary layer separates before 55%chord, a constant pressure region appears in the pressure distribution curves after separation, and later at the aft portion of the blade the flow reattaches to the airfoil surface. The constant pressure region formed on the pressure distribution curves show that a separation bubble forms over the suction surface of the airfoil. This behaviour is a typical character of an airfoil operating at low Reynolds numbers when separation occurs. In addition, as seen in the figure, as the Reynolds number decreases flow reattachment occurs further downstream forming a larger separation bubble on the surface. In addition, since transition onset is defined as the point where a sudden pressure recovery appears on the pressure distribution curve, it can be said that the transition onset points also moves downstream as the Reynolds number decreases.

3.3.2 Boundary Layer Measurements with Hot-Wire Anemometry

Under the same operating conditions with C_p measurements, hot-wire anemometry measurements are conducted at several chordwise locations in order to better resolve the flow dynamics within the separated boundary layer for the baseline cases. Measurements are performed at3.25 cm away from the mid-span; in other words, a few cm nearer to one of the tunnel walls in order to be able to compare current hot wire data with the Particle Image Velocimetry Measurements (PIV) over the blade. Since the tunnel test section is very big it is hard to focus the high speed camera to a certain region over the mid span of the blade for PIV measurements. Thus, in order to enable PIV measurements at the same spanwise location with the hot wire measurements, current hot wire measurements are conducted 3.25 cm away from the mid span. Conducted preliminary PIV measurements show that this distance is suitable for camera focusing.

Before starting the discussion on the boundary layer quantities, it is worth to underline some general points about the hot wire measurements. First of all, hot wire does not have the ability to sense the direction of the flow. Hot wire just measures the magnitude of the flow passing over the thin wire. Therefore, the reverse flow cannot be distinguished directly from the mean velocity data. In addition, hot wire measures higher mean velocities than the actual ones when there are high turbulent fluctuations in the flow with near zero mean velocity. With these facts in mind the following boundary layer quantities obtained from the hot wire measurements can be analysed and discussed better.

Re= $3.4x10^5$ and Re=$5.1x10^5$ cases

In this part, boundary layer characteristics of the S809 airfoil at low Reynolds number is analysed at two different Reynolds numbers, namely $3.4x10^5$ and $5.1x10^5$, at zero angle of attack.

Figure 3.3.2, Figure 3.3.3, Figure 3.3.4 and Figure 3.3.5, demonstrate mean and fluctuating velocity profiles and at several chordwise locations at two Reynolds numbers, namely $3.4x10^5$ and $5.1x10^5$, at zero angle of attack. Mean velocities and fluctuating velocities (called also turbulent fluctuations) are normalized by the mean edge velocity of the local boundary layer and wall normal distance is normalized by local chord location. Wall normal distance is the vertical distance traversed from the airfoil surface in the direction of the local boundary layer thickness and the local chord is the chordwise distance from the leading edge of the airfoil to the measurement location. Also, it should be noted that the measured velocities are axial velocities, thus, before calculating the boundary layer quantities, at each traverse location they are transformed to the local airfoil coordinates.

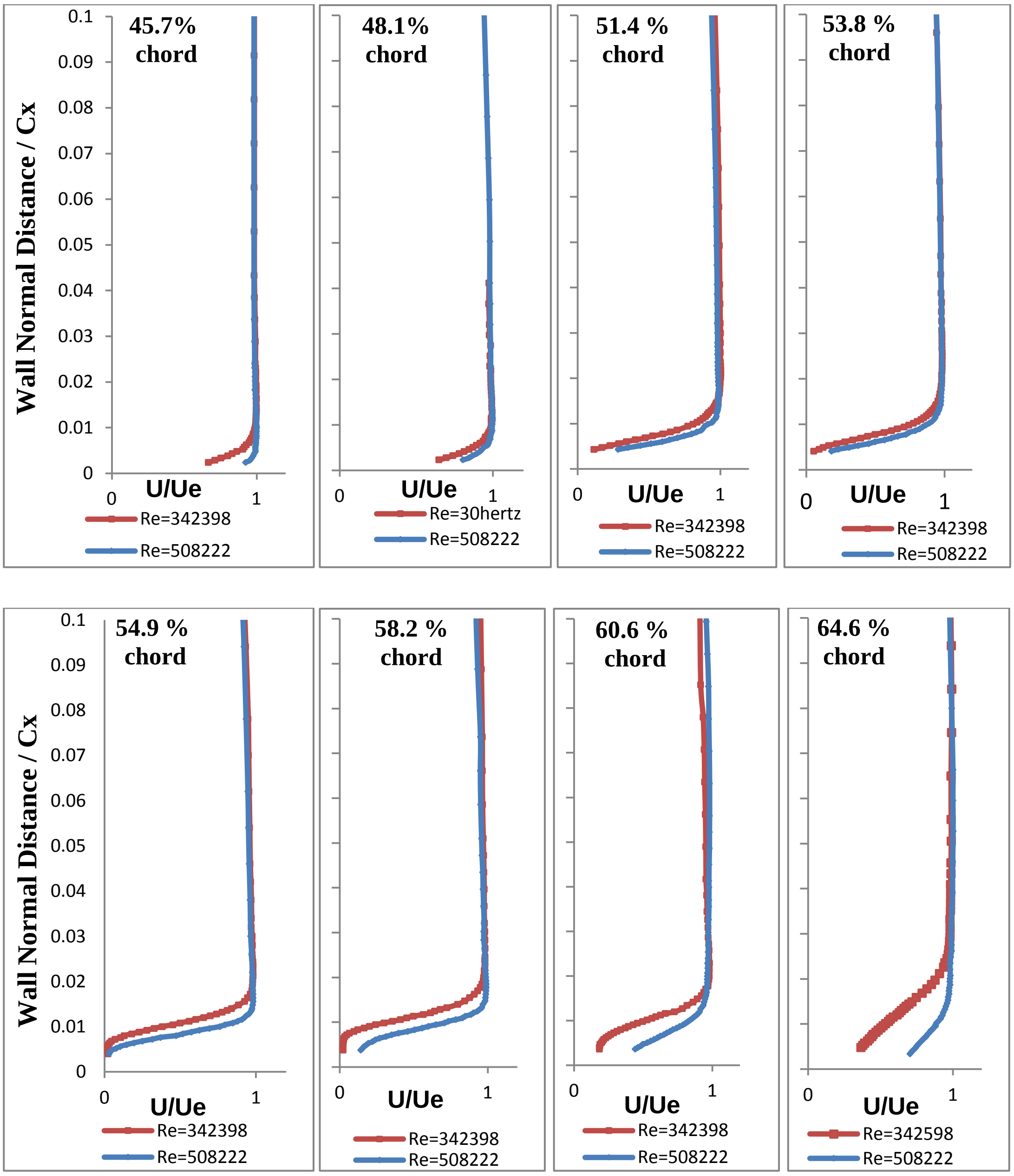

Figure 3.3.2: Mean velocity profiles at several chordwise locations for the Reynolds numbers of $3.4x10^5$ and $5.1x10^5$, at zero angle of attack.

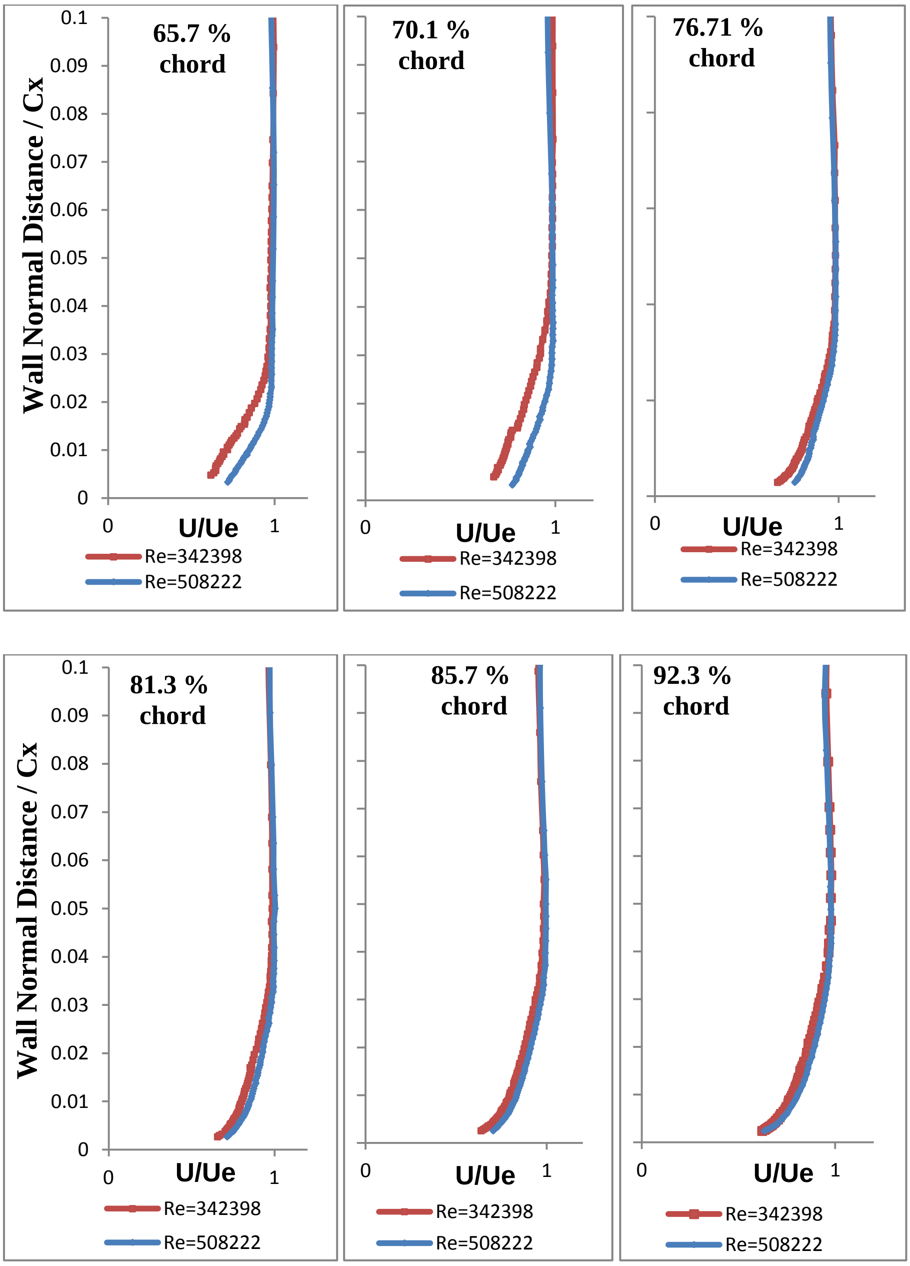

Figure 3.3.3: Mean velocity profiles at several chordwise locations for the Reynolds numbers of $3.4x10^5$ and $5.1x10^5$, at zero angle of attack.

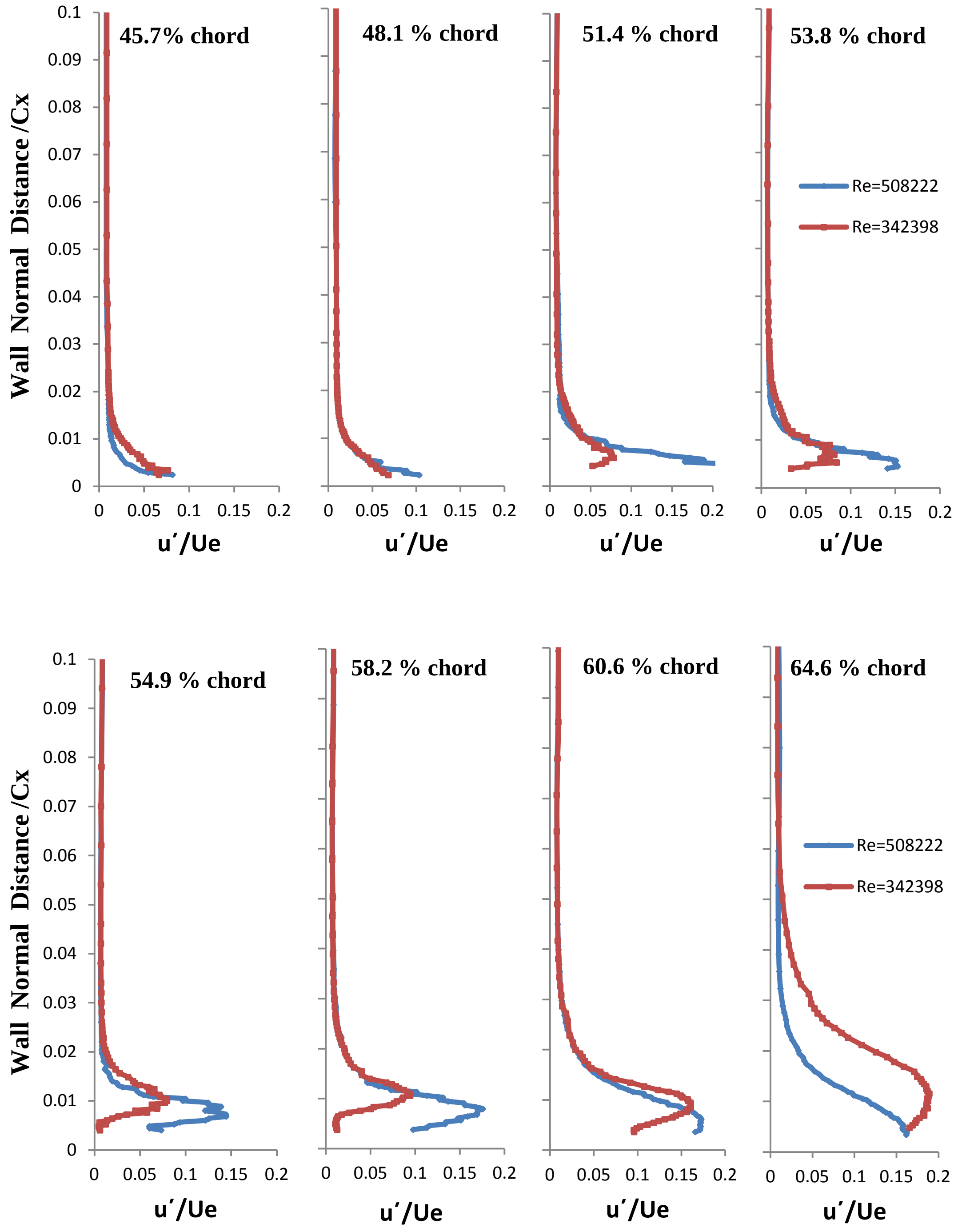

Figure 3.3.4: Fluctuating velocities (turbulent fluctuations) at several chordwise locations for the Reynolds numbers of 3.4×10^5 and 5.1×10^5, at zero angle of attack.

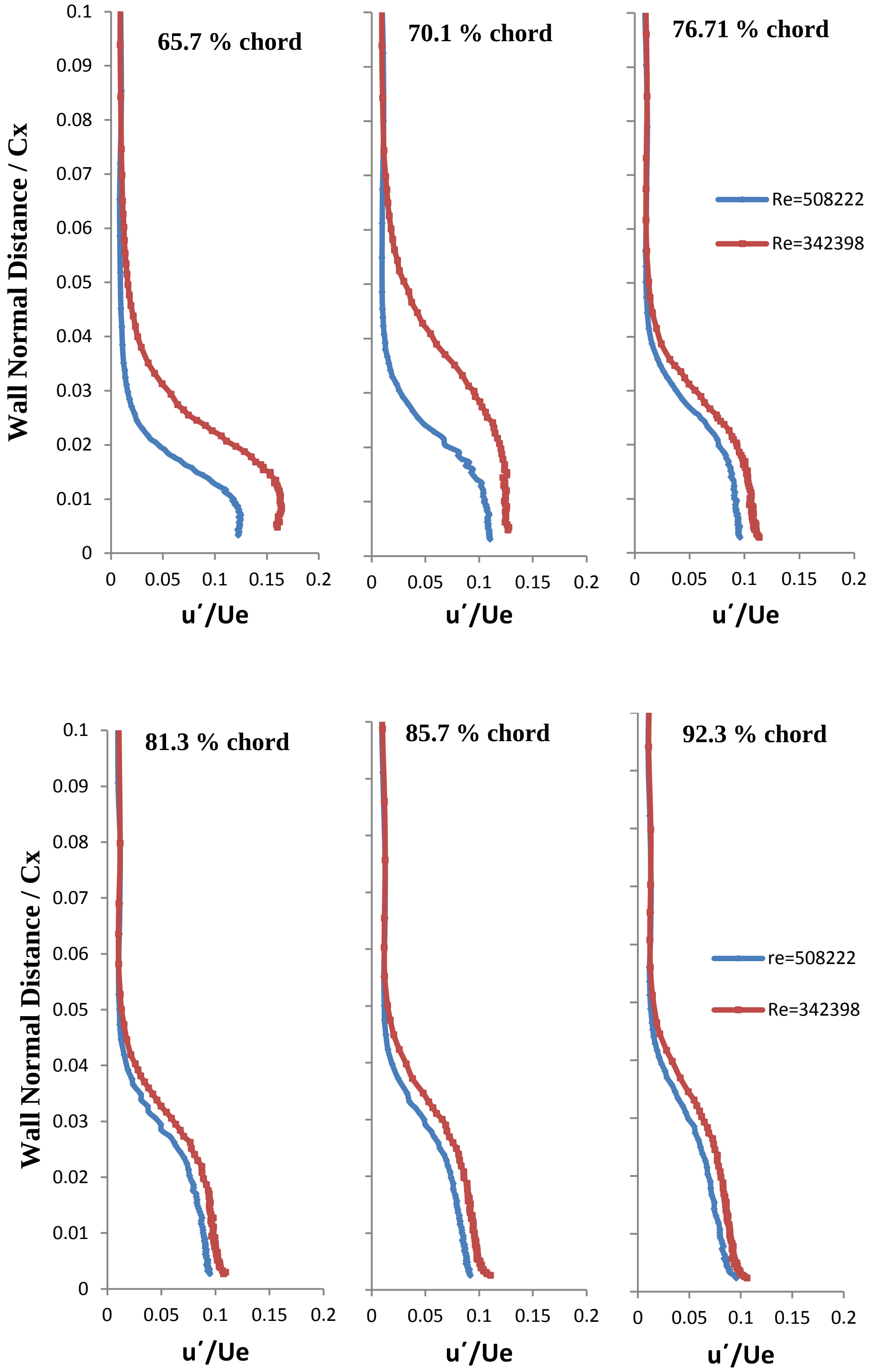

Figure 3.3.5: Fluctuating velocities (turbulent fluctuations)at several chordwise locations for the Reynolds numbers of $3.4x10^5$ and $5.1x10^5$, at zero angle of attack.

From the mean velocity profiles it is observed that at 45.7% and 48.1% chord locations, mean velocity profiles at both Reynolds numbers are laminar with no inflection points. Also, the turbulent fluctuations are quite low at these traverse locations at these Reynolds numbers. At the third traversed location, namely 51.4% chord location, at these two Reynolds numbers, an inflection point is clearly visible in the mean velocity profiles, and the turbulent fluctuations are quite higher than the previous traverse location. This means that the flow has separated somewhere between 48.1% and 51.4% chord locations, and this conclusion is compatible with the surface pressure measurements. After that chord location some differences occur between these two low Reynolds number flows. For the $3.4x10^5$Reynolds number case, after the separation, inflection points become more visible in the mean velocity profiles at 53.8%, 54.9%, 58.2%, 60.6% and 64.6% chord locations, which means flow is still separated. Turbulent fluctuations, on the other hand, continue increasing both in the streamwise direction and in the normal direction (along the boundary layer thickness). However, near the wall (airfoil surface), the behaviour of the turbulent fluctuations is different. Downstream the separation zone, in a region including 53.8%, 54.9% and 58.2% chord locations, turbulent fluctuations near the wall is quite low and the mean velocities are very close to zero. This may be attributed to a dead air region inside the laminar separation bubble. After this dead air region, turbulent fluctuations and mean velocities increase again near the wall. This increase is probably due to a reverse vortex flow inside the bubble. An increase in velocity fluctuations near the airfoil surface between 58.2%-60.6% chord stations indicate that transition begins between these stations. With the 65.7% chord location, no inflection is seen in the mean velocity profiles and similarly there is no peak fluctuation in the turbulent fluctuation profiles any more. Also, 65.7% chord station has the maximum turbulent fluctuations. This means flow reattachment begins around 65.7% chord. For the $5.1x10^5$ Reynolds number case, although flow development within the separated boundary layer is similar, it is seen that the dead air region is much smaller and flow reattachment occurs earlier. Based on the figures it is seen that reattachment occur around 64.6% chord locations, forming a smaller separation bubble.

Re= $2.3x10^5$ case

Since the flow dynamics within the separated boundary layer at $2.3x10^5$ Reynolds number is detected better and laminar separation bubble is observed to be larger, this case is analysed and discussed in detail in this part. Also, because of the same reasons, active flow control using the synthetic jet actuators is studied on the airfoil at this Reynolds number.

In order to resolve the flow development within the boundary layer, mean and fluctuating velocity profiles along with the turbulence intensity levels are determined at several chordwise locations based on the hot wire measurements, and the resultant data is demonstrated in the following figures.

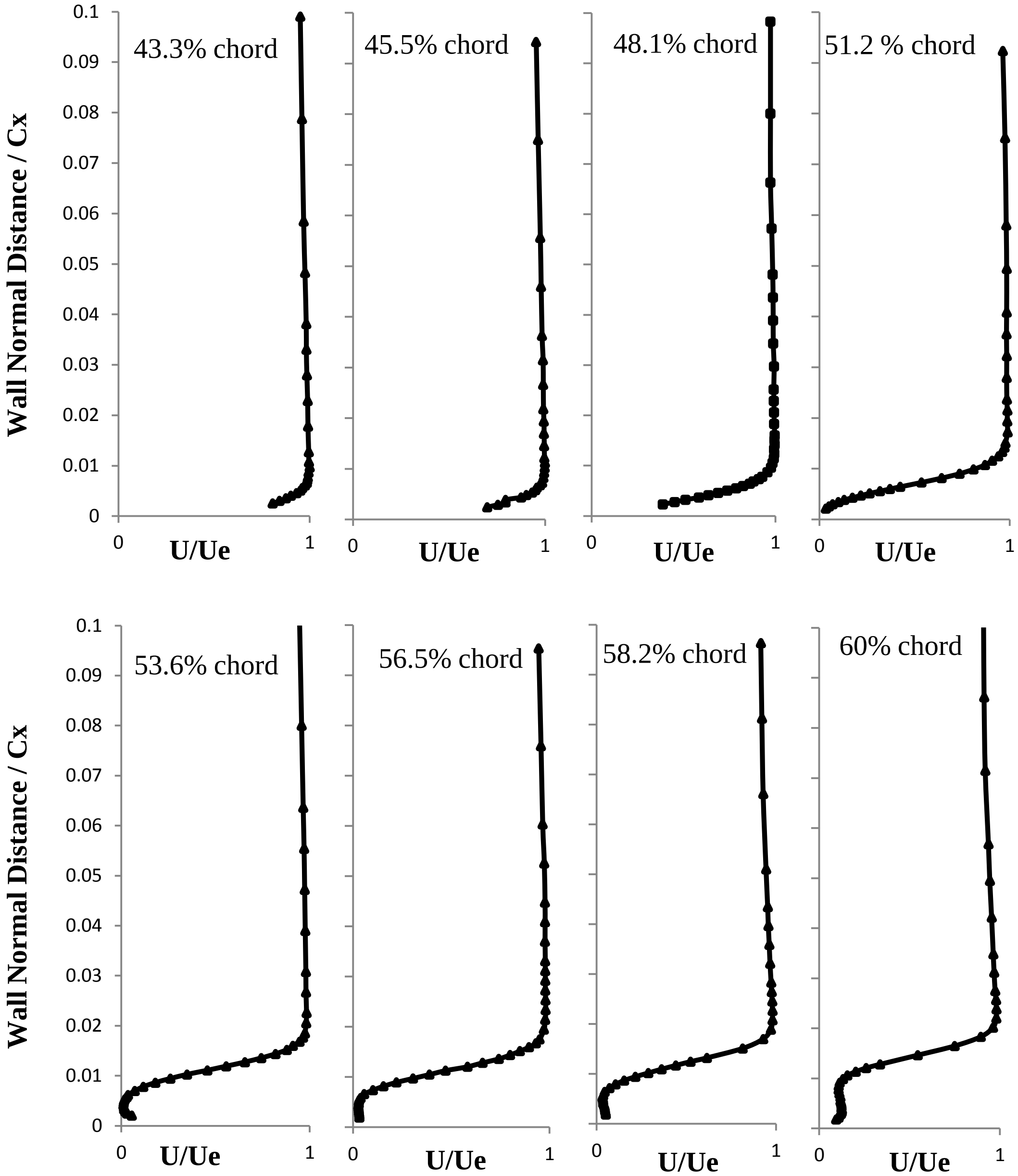

Figure 3.3.6: Mean velocity profiles at several chordwise locations at $2.3x10^5$ Reynolds number, at zero angle of attack.

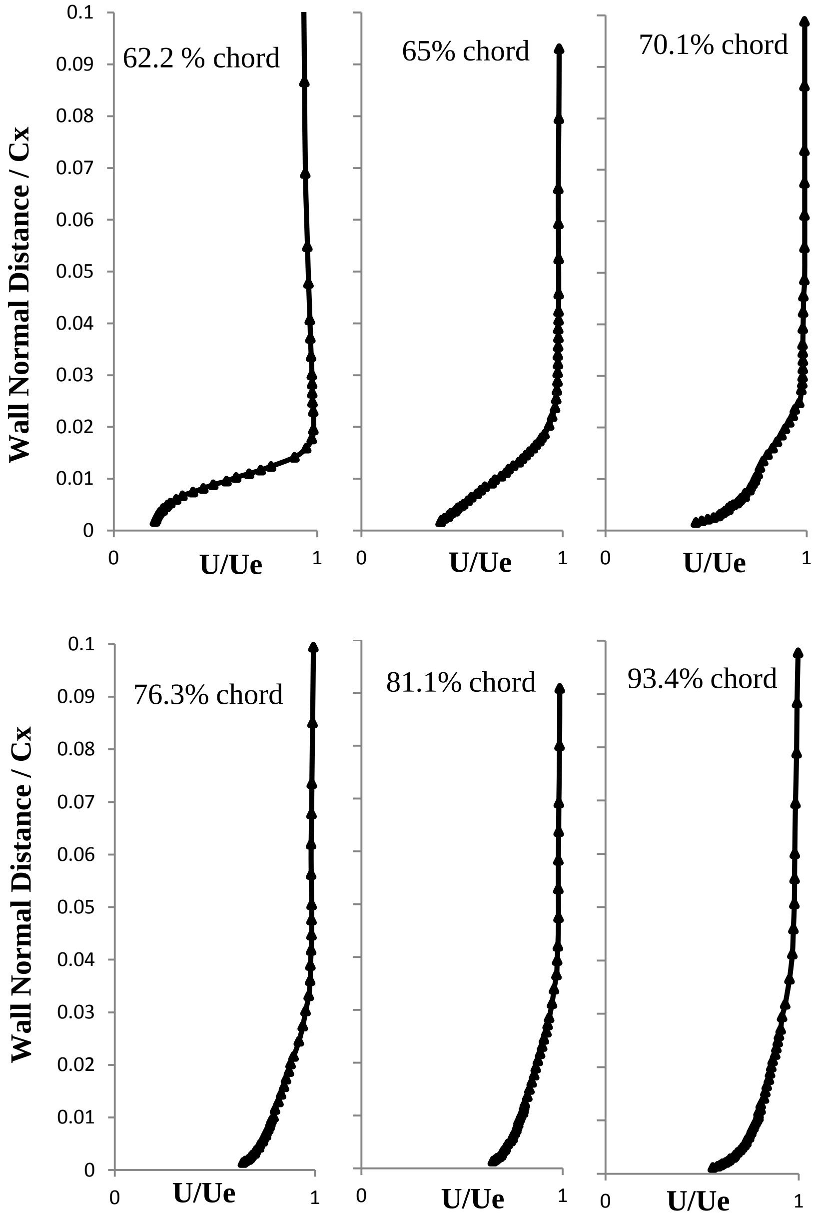

Figure 3.3.7: Mean velocity profiles at several chordwise locations at 2.3×10^5 Reynolds number, at zero angle of attack.

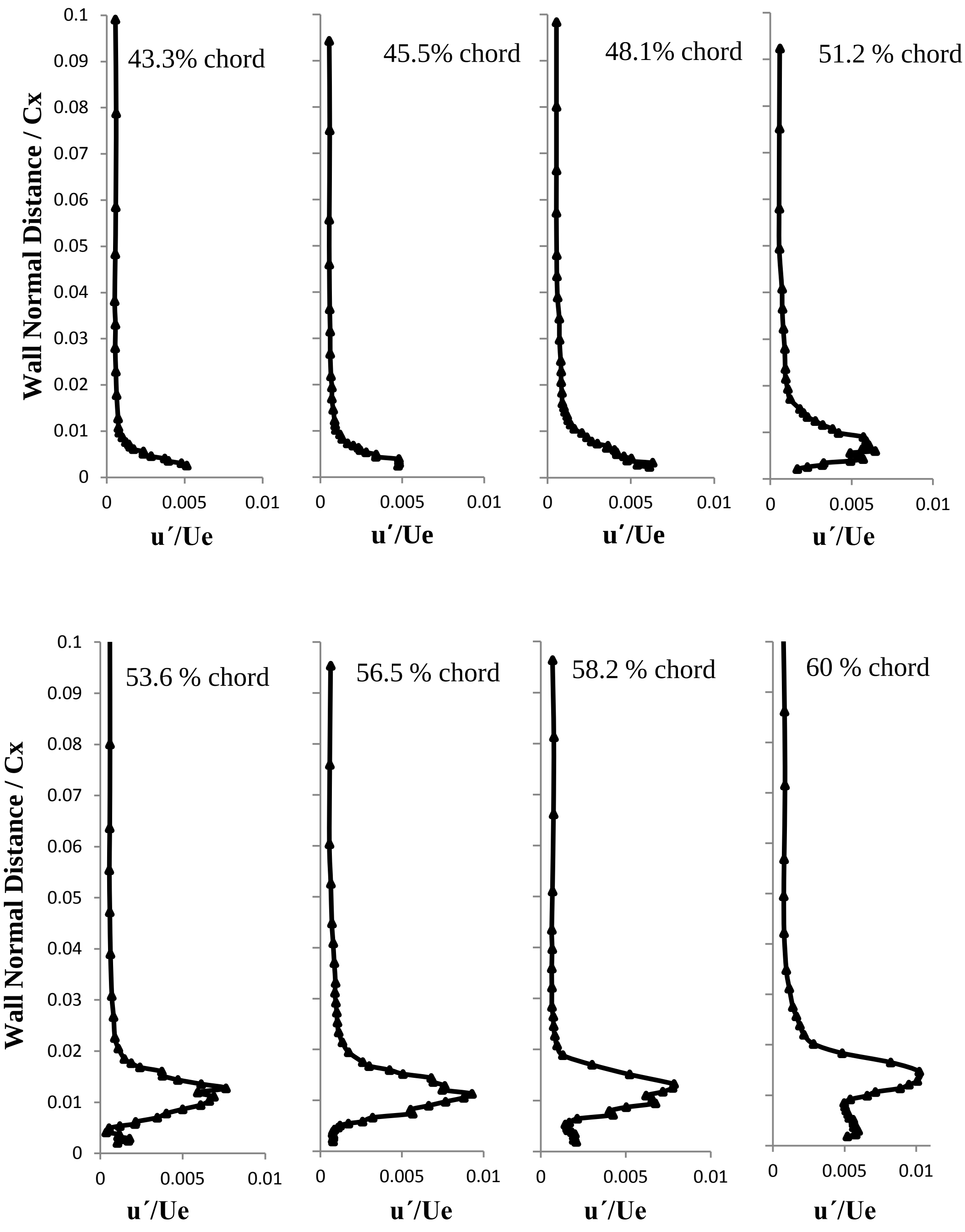

Figure 3.3.8: Fluctuating velocity profiles (turbulent fluctuations) at several chordwise locations at $2.3x10^5$ Reynolds number, at zero angle of attack.

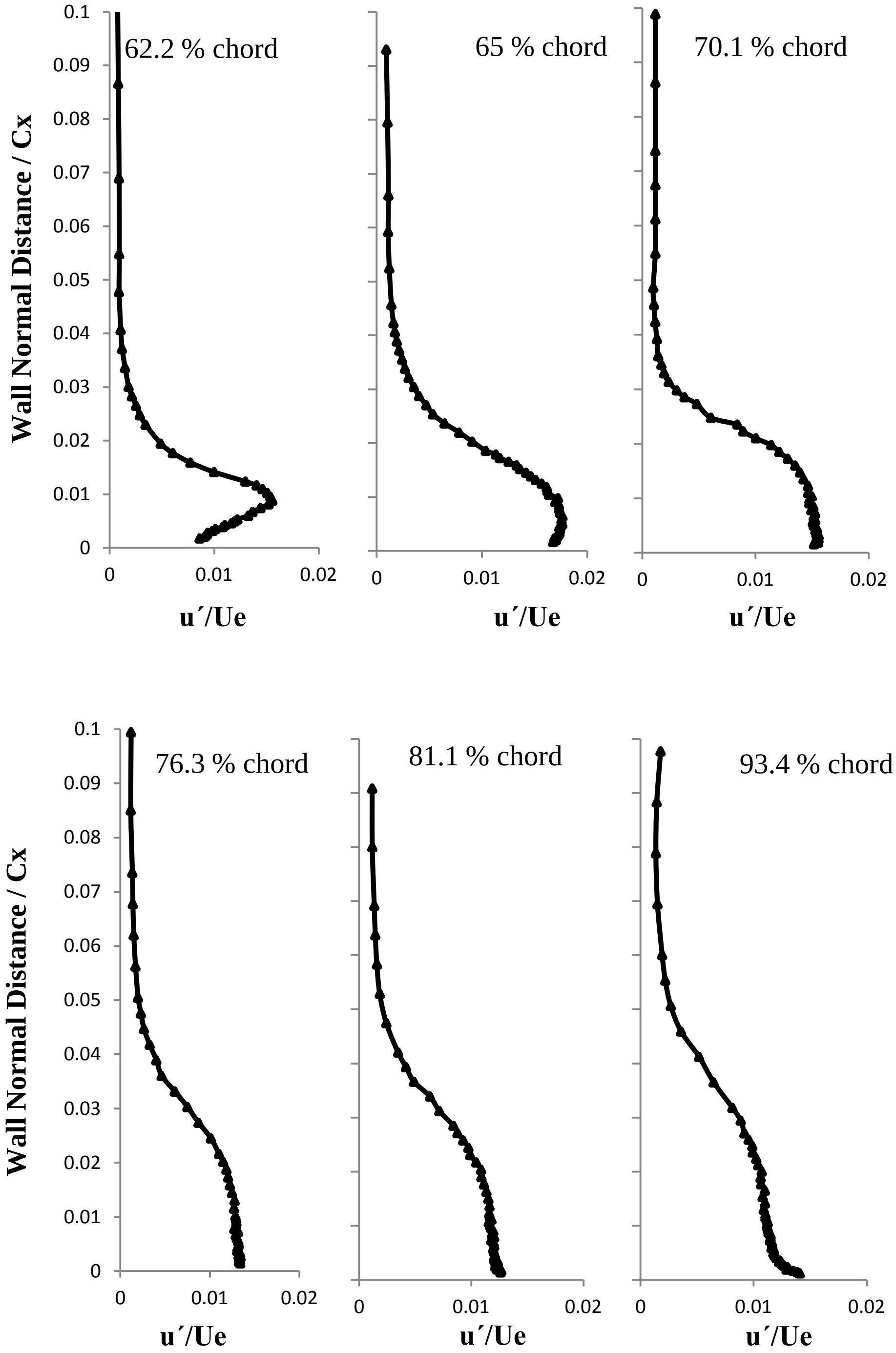

Figure 3.3.9: Fluctuating velocity profiles (turbulent fluctuations) at several chordwise locations at 2.3×10^5 Reynolds number, at zero angle of attack.

The mean velocities and the fluctuation velocities are normalized by local edge velocity of the boundary layer. Similarly, wall normal distance is normalized by the local chord distance. From theFigure 3.3.6, no inflection point is detectable in the mean velocity profiles at 43.3% and 45.5% chord locations. Also, the velocity profile is linear near the wall and fluctuating velocity components (turbulent fluctuations) at these locations are low as seen in theFigure 3.3.8. Therefore, the flow is laminar and has not separated yet. At 48.1% traverse location, although an inflection point is not clearly visible in the mean velocity profile the fluctuating velocity level is higher than the fluctuations at the previous traverse location, 45.5% chord. This may be an indication of laminar separation around this location. At the 51.2% chord location, on the other hand, an inflection point away from the wall is clearly visible in the mean velocity profile. Also, a higher amount of turbulent fluctuations are detectable at this location as demonstrated in theFigure 3.3.8. These indications ensure that this location is on the downstream of the laminar separation point. In addition, downstream the separation point, it is observed that turbulent fluctuations increase both in the streamwise direction and normal directions. However, near the wall (airfoil surface), there occurs a region with near zero mean and fluctuating velocities. This is an indication of a dead air region where the flow is almost stationary within the separated shear layer. Traverse locations on the 51.2%, 53.6%, 56.5% and 58.2% chord seem to be inside or very close to this stationary flow region. Downstream the dead air region both the mean velocities and turbulent fluctuations increase again near the wall, which may be attributed to the presence of a strong recirculation region which is known to cause a strong momentum exchange between the free stream and the flow within the separated shear layer and therefore, to cause the separated shear layer to reattach to the surface again. Burgmann and Schröder (2008) state that due to the disturbances within the boundary layer, shear layer rolls up downstream and this process, at the rear of the separation bubble, generates vortices which causes fluid transformation towards the wall and away from the wall on the downstream and on the upstream of the vortex, respectively[41].Although hot-wire does not provide the direction of the flow, from the mean velocity profile at the 60% chord location, a reverse flow is clearly identified. This ensures the presence of a strong recirculation region around there. After the65% chord location, it is seen that the peaks in the fluctuating velocity profiles disappears, also, fluctuating velocities are almost constant near the wall, which is an indication of flow reattachment between 65% and 70.1% chord station. With the reattachment, a laminar separation bubble occurs within the boundary layer and it is seen that flow develops downstream with fuller mean velocity profiles near wall which is a typical behaviour of turbulent boundary layer flows.

In the study of McAuliffe, maximum turbulent fluctuations (maximum velocity fluctuations) were observed to be corresponding to inflection points in the mean velocity profiles of the laminar separated shear layer [42]. From the above figures, it is seen that peak fluctuating velocities occur near inflection points in the mean velocity profiles. Therefore, based on the maximum turbulent fluctuations in theFigure 3.3.8 and Figure 3.3.9, inflection points in the mean velocity profiles can be estimated.

Moreover, as proposed by McAuliffe [42], since near zero mean velocity turbulence intensities are very high, turbulence intensity profiles can give an insight about the location of zero mean velocities in the boundary layer.Figure 3.3.10 and Figure 3.3.11show the turbulence intensity levels normalized by local mean velocity.

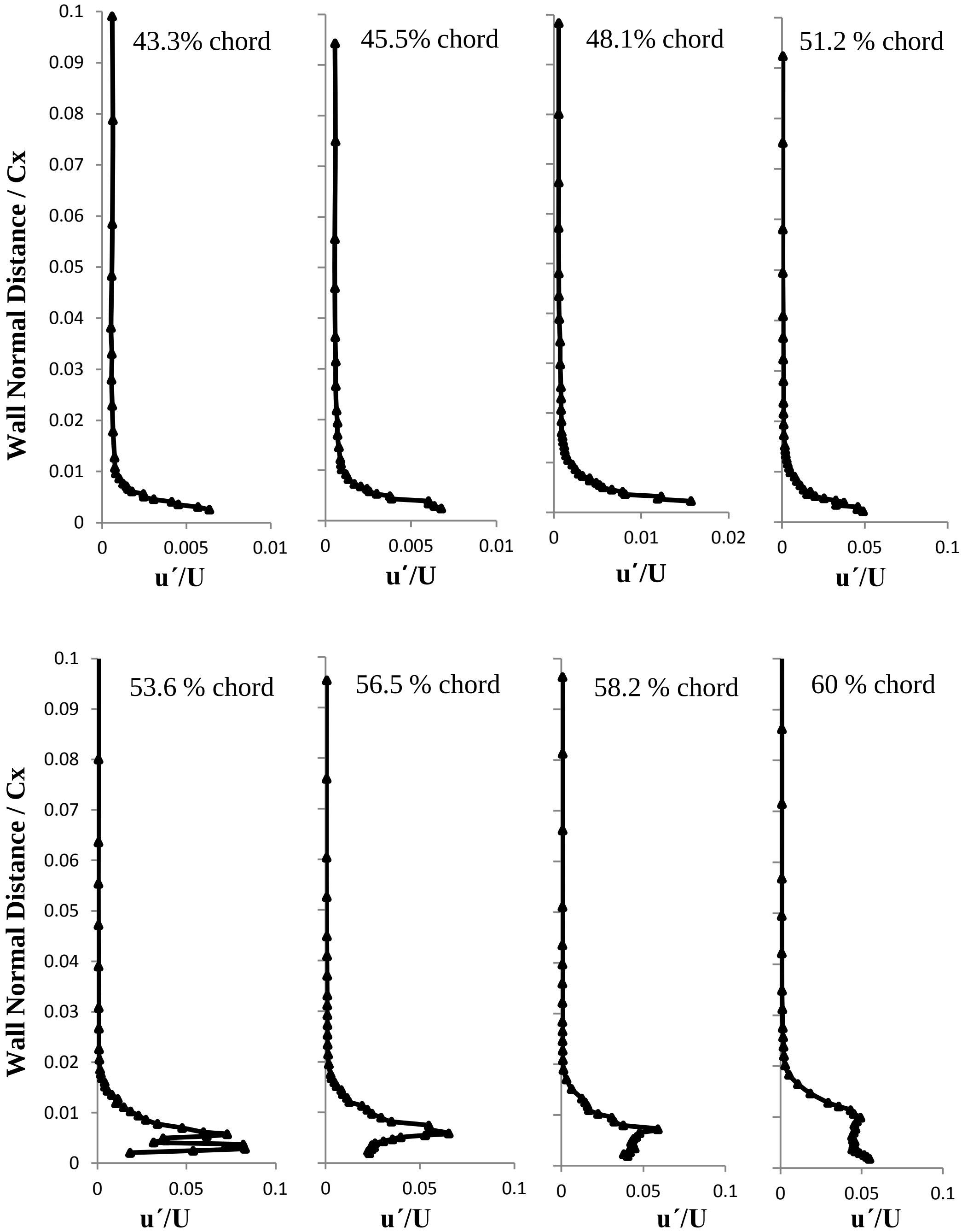

Figure 3.3.10: Turbulence intensity profiles at several chordwise locations at $2.3x10^5$ Reynolds number, at zero angle of attack.

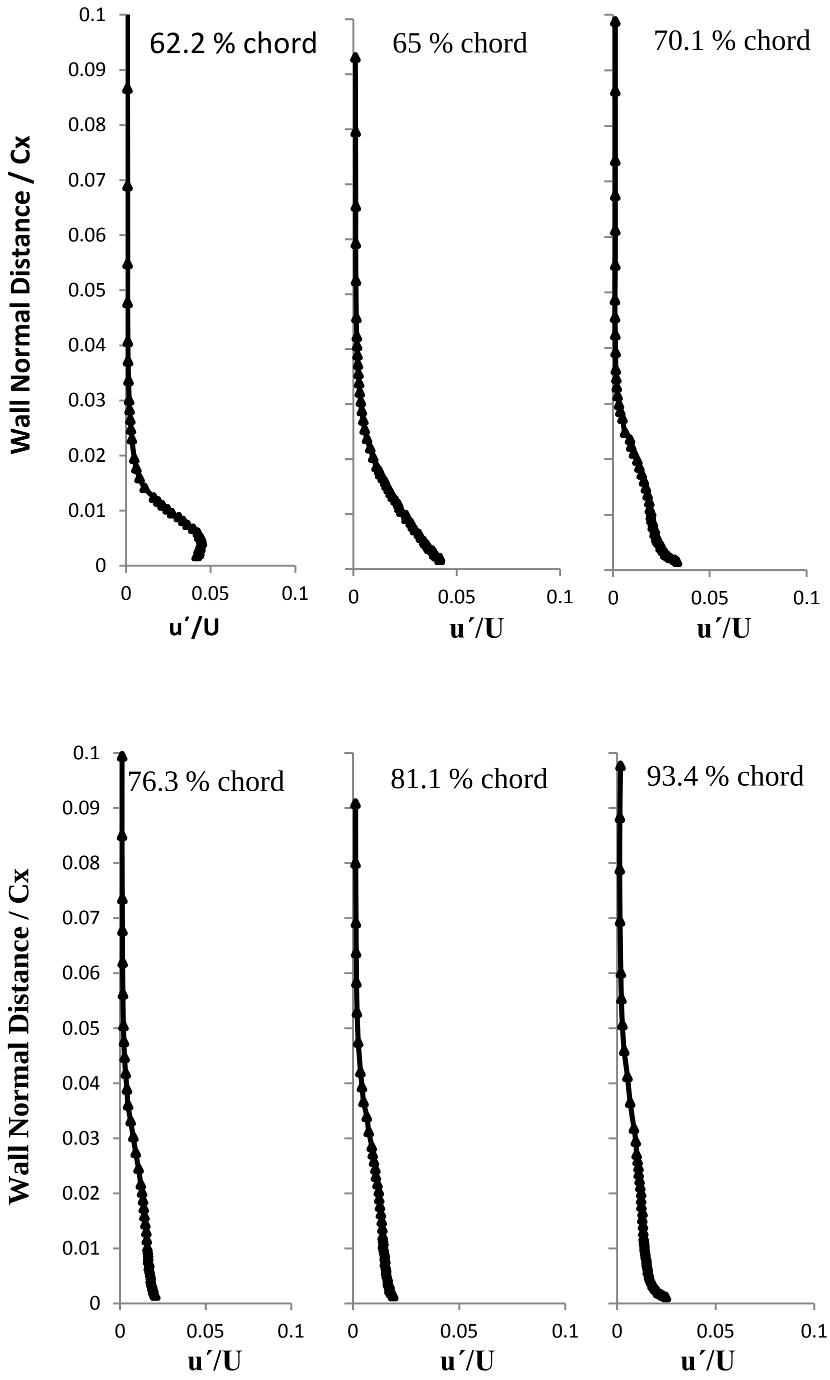

Figure 3.3.11: Turbulence intensity profiles at several chordwise locations at $2.3x10^5$ Reynolds number, at zero angle of attack.

Figure 3.3.10 and Figure 3.3.11show that upstream the separation point, which was found to be around 48.1% chord location, the maximum turbulence intensities occur on the wall, which indicates that there is no zero mean velocity in the boundary layer; therefore, no separation. On the other hand, downstream the separation point, the peaks in the turbulence intensity profiles become visible and appear away from the surface. As the separated shear layer develops downstream the distance of the peak turbulence intensities from the wall also increases until 60% chord location. After this chord location the peaks start to come closer to the wall again and with the 65% chord location no peak appears in the profile away from the surface anymore. Also, the turbulence intensities are observed to decrease 70.1% chord station. Therefore, it can be concluded that the flow reattachment starts somewhere between 65% and 70.1% chord. As seen the interpretation of the turbulence intensity profiles support the discussions made based on the mean and fluctuating velocity profiles in the previous part.

3.3.3 2D Particle Image Velocimetry (PIV) Measurement Results for 2.3×10^5 Reynolds number case

Due to a problem with the Litron laser of the PIV system, only baseline case measurements (at 2.3×10^5 Reynolds number) are conducted. Following figures demonstrates 2D time resolved PIV results.

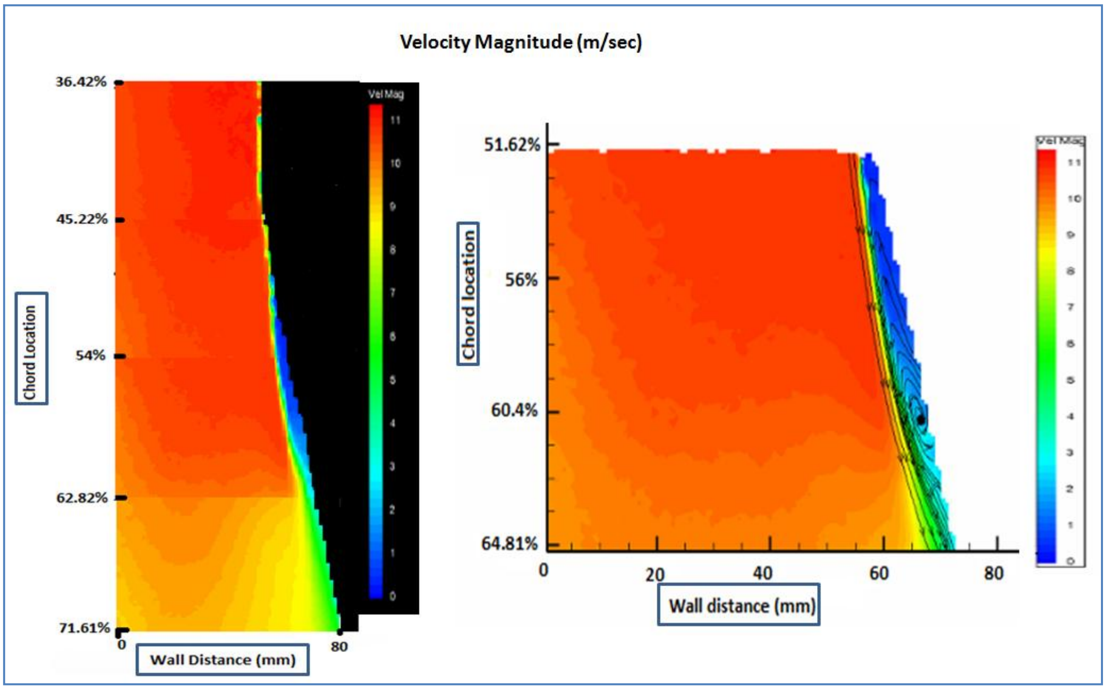

Figure 3.3.12:Velocity Magnitudes showing the laminar separation bubble over the airfoil surface.

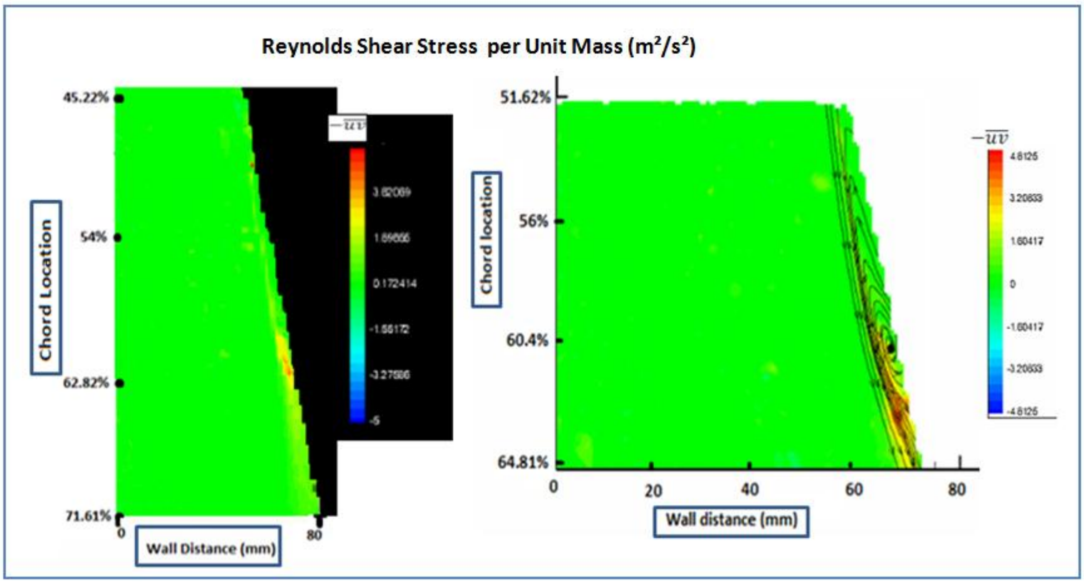

Figure 3.3.13:Reynolds stress stresses per unit mass around the laminar separation bubble over the airfoil surface.

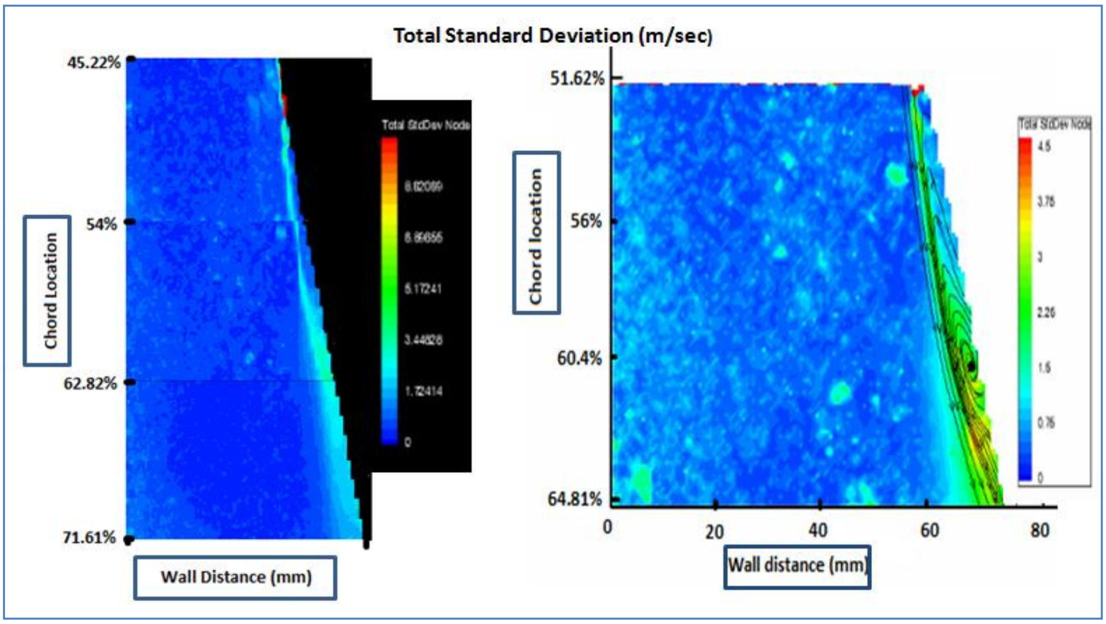

Figure 3.3.14: Total velocity standard deviation levels around the laminar separation bubble over the airfoil surface.

From the velocity contours inFigure 3.3.12, it is seen that flow separates around 48% chord location, and with the reattachment detected a laminar separation bubble forms over the airfoil. Within the separation bubble, the dead air zone, the strong recirculation zone and the formation of vortical structure around 61% chord location is clearly visible. Since a rapid increase in Reynolds shear stress is an indication of the location of transition onset, from theFigure 3.3.13, it is seen that transition begins around 58% chord station. Similarly, total standard deviation levels increases rapidly in the strong recirculation region as observed in Figure 3.3.14and gets maximum at around 63.5% chord. The maximum deviation shows the location of the first reattachment point within the separated shear layer.

Some general conclusions can be drawn about the flow development within the boundary layer over the S809 airfoil at these three Reynolds numbers based on the mean and fluctuating velocity profiles, PIV measurements and surface pressure distributions. First of all, it is seen that the results of the surface pressure, hot wire and PIV measurements are in good agreement with each other. Second, it is detected that as the Reynolds number increases transition and reattachment onsets come forward; that is, high Reynolds numbers accelerate flow development within the separated shear layer. As a result, a shorter separation bubble forms for higher Reynolds numbers. Third, the effect of the Reynolds number on the separation point is not clearly determined; but, the separation points at these three Reynolds numbers seem to be close to each other. Finally, although more detailed PIV analysis should be conducted in order to determine the exact location of the separation, transition and reattachment points, the measurements and results help to understand the behaviour of the flow within the separated shear layer.

3.3.4 Synthetic Jet Actuator (SJA) Case

Baseline case for S809 airfoil is analyzed and discussed in detail in the previous part. Now, in this part, experimental results for the controlled case are presented and the effect of the periodic excitation generated by synthetic jet actuators on the laminar separation bubble and the flow development in the wake at 2.3×10^5 Reynolds number is examined and discussed. The array of synthetic jet actuators mounted at the 28% chord location in the mid span of the S809 blade consists of three individually controlled actuators, and they are flush mounted on the surface of the blade. Each synthetic jet has a rectangular orifice with a width of 0.5 mm and a length of 10 mm and they are spaced 27.37 mm apart. Details of the synthetic jet actuator configuration and measurement details can be found in Chapter2.

During the controlled case experiments synthetic jet actuators are driven with a sinusoidal actuation of 1450 Hz and 300Vp-p.

<u>Boundary Layer Analysis</u>

In order to resolve the effect of the periodic excitation generated from the synthetic jet actuators on the flow development within the boundary layer, mean and fluctuating velocity profiles along with the turbulence intensity levels are determined at the same chordwise locations based on the hot wire measurements, and the results are presented together with the uncontrolled case profiles in the following figures

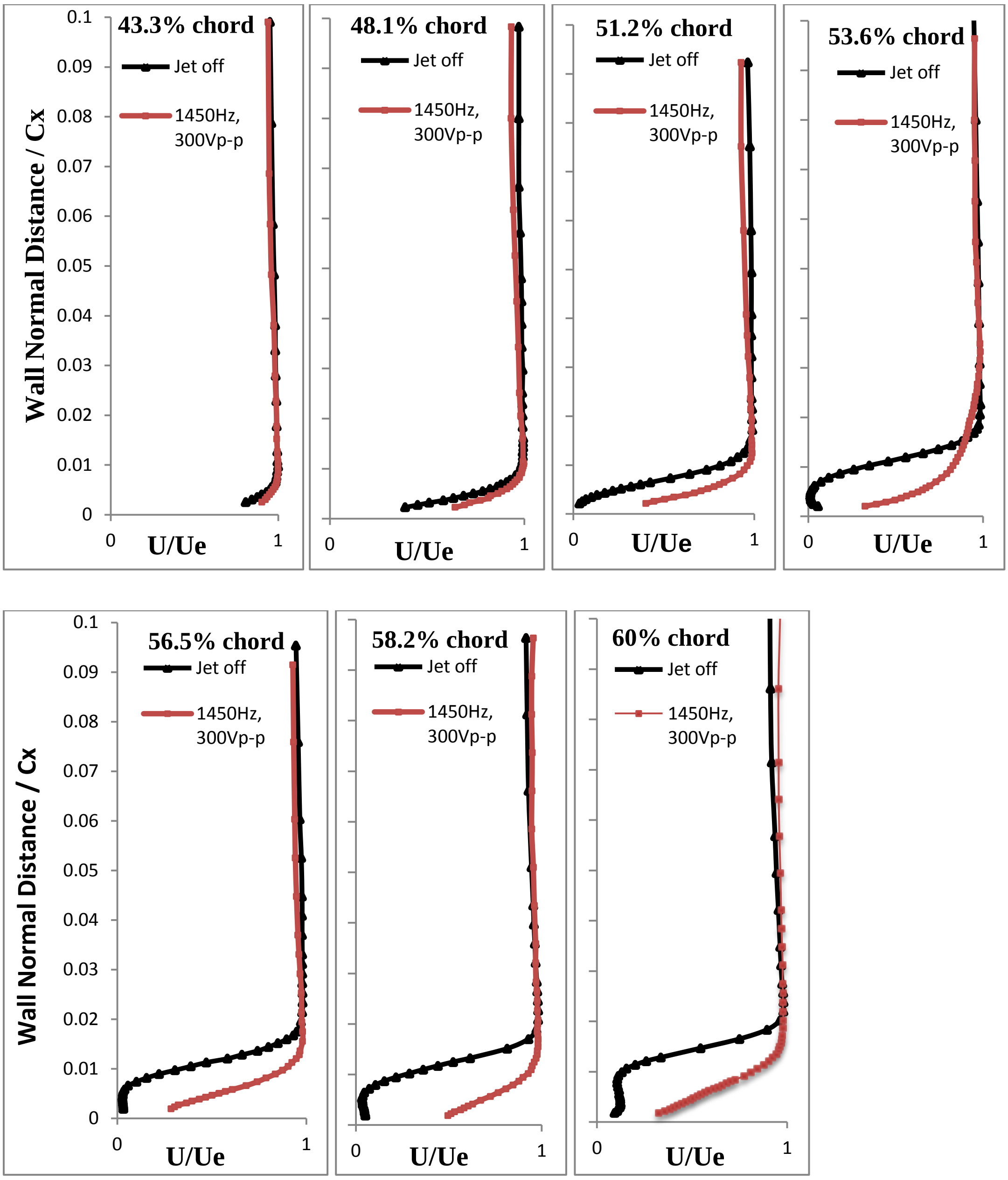

Figure 3.3.15:Mean velocity profiles at several chordwise locations at 2.3x10^5 Reynolds number, at zero angle of attack.

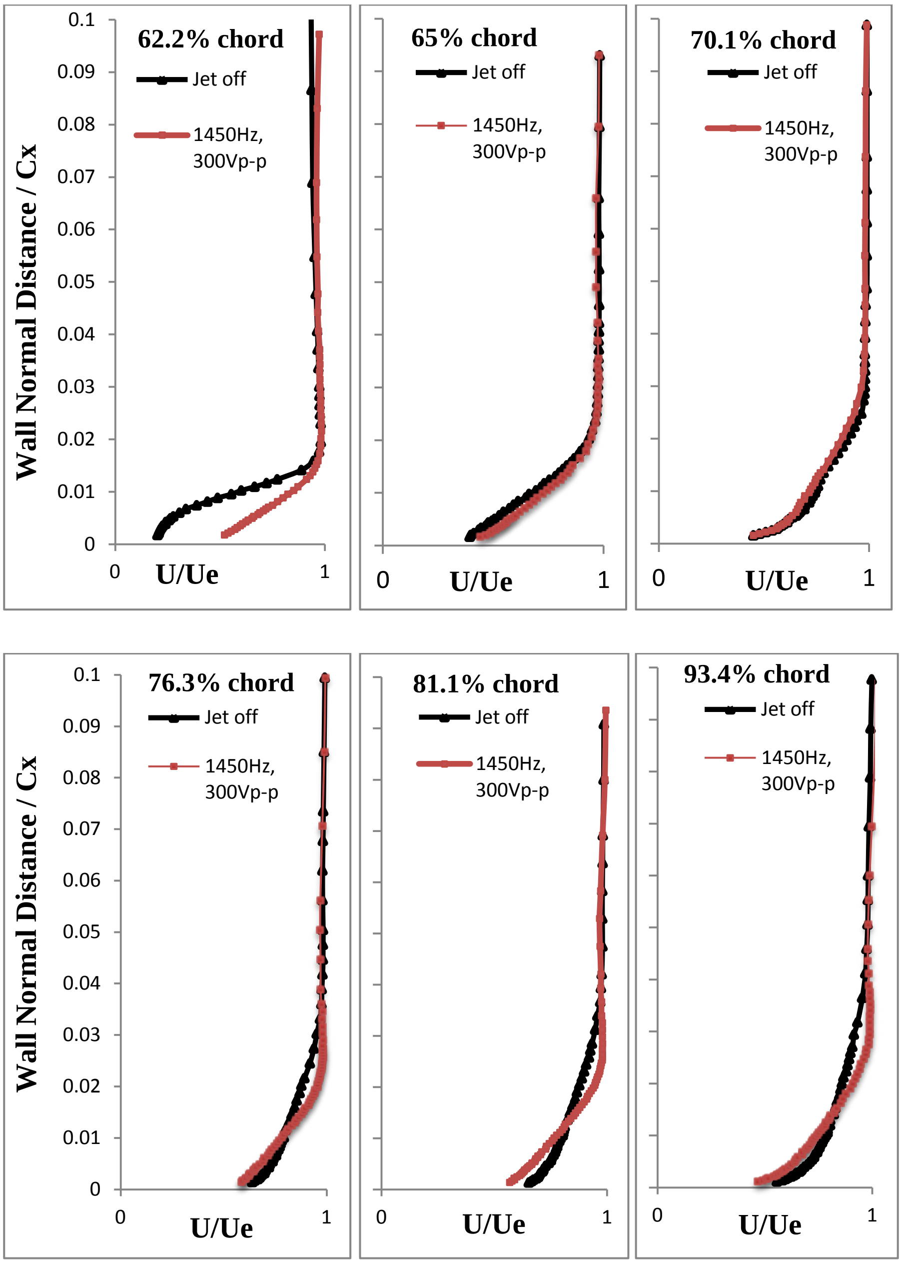

Figure 3.3.16: Mean velocity profiles at several chordwise locations at $2.3x10^5$ Reynolds number, at zero angle of attack.

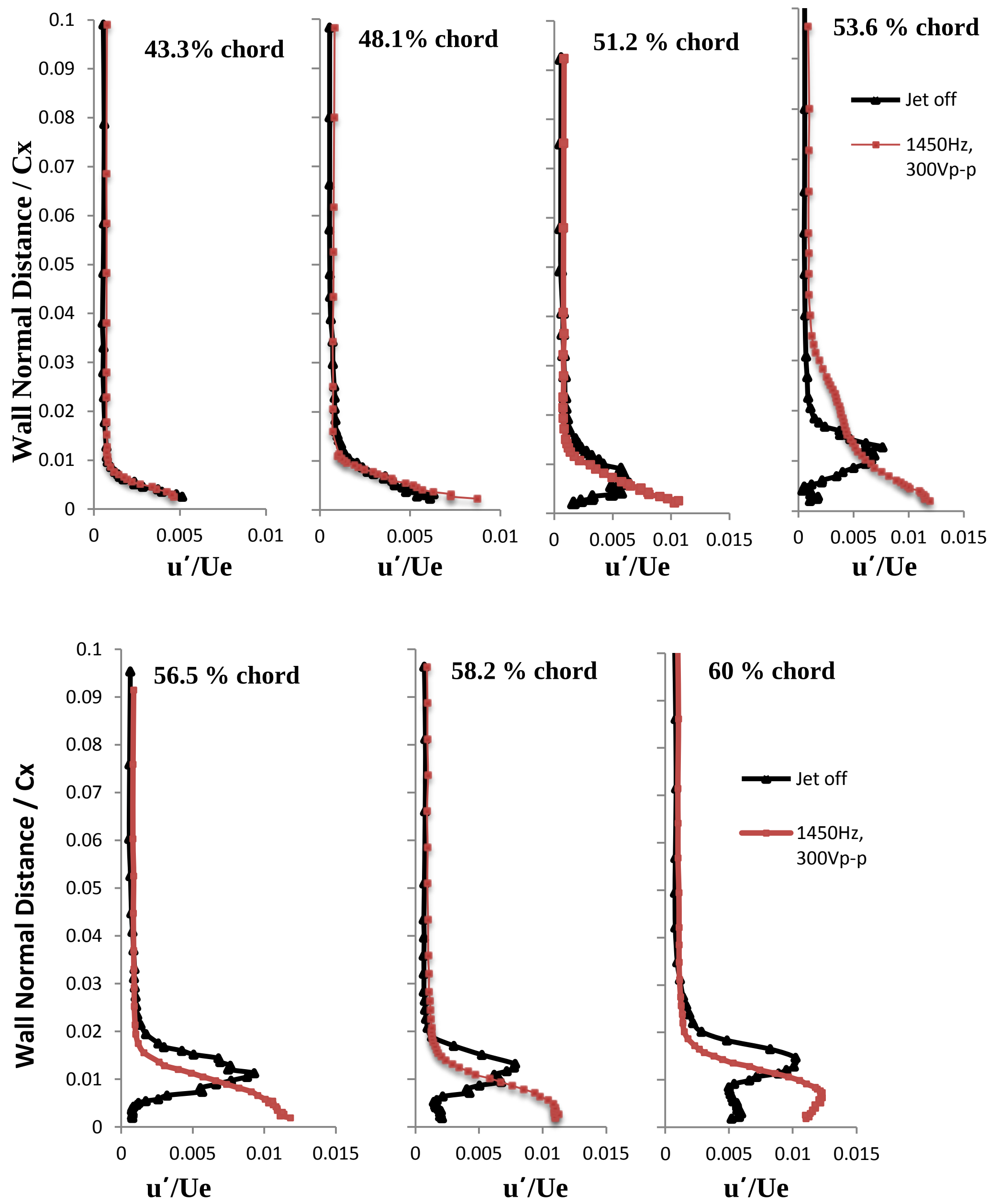

Figure 3.3.17: Fluctuating velocity profiles at several chordwise locations at 2.3×10^{5} Reynolds number, at zero angle of attack.

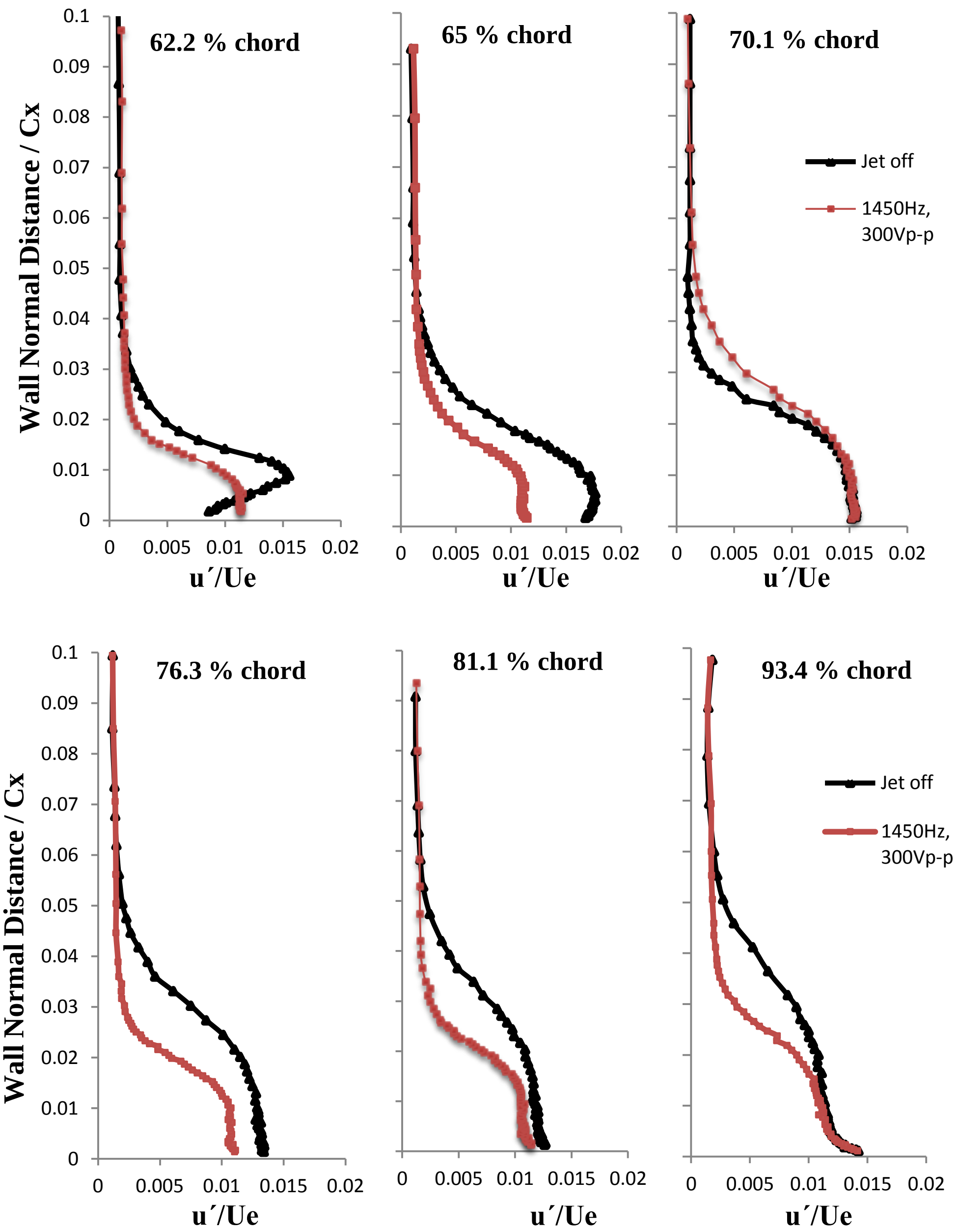

Figure 3.3.18: Fluctuating velocity profiles at several chordwise locations at 2.3x10^{5} Reynolds number, at zero angle of attack.

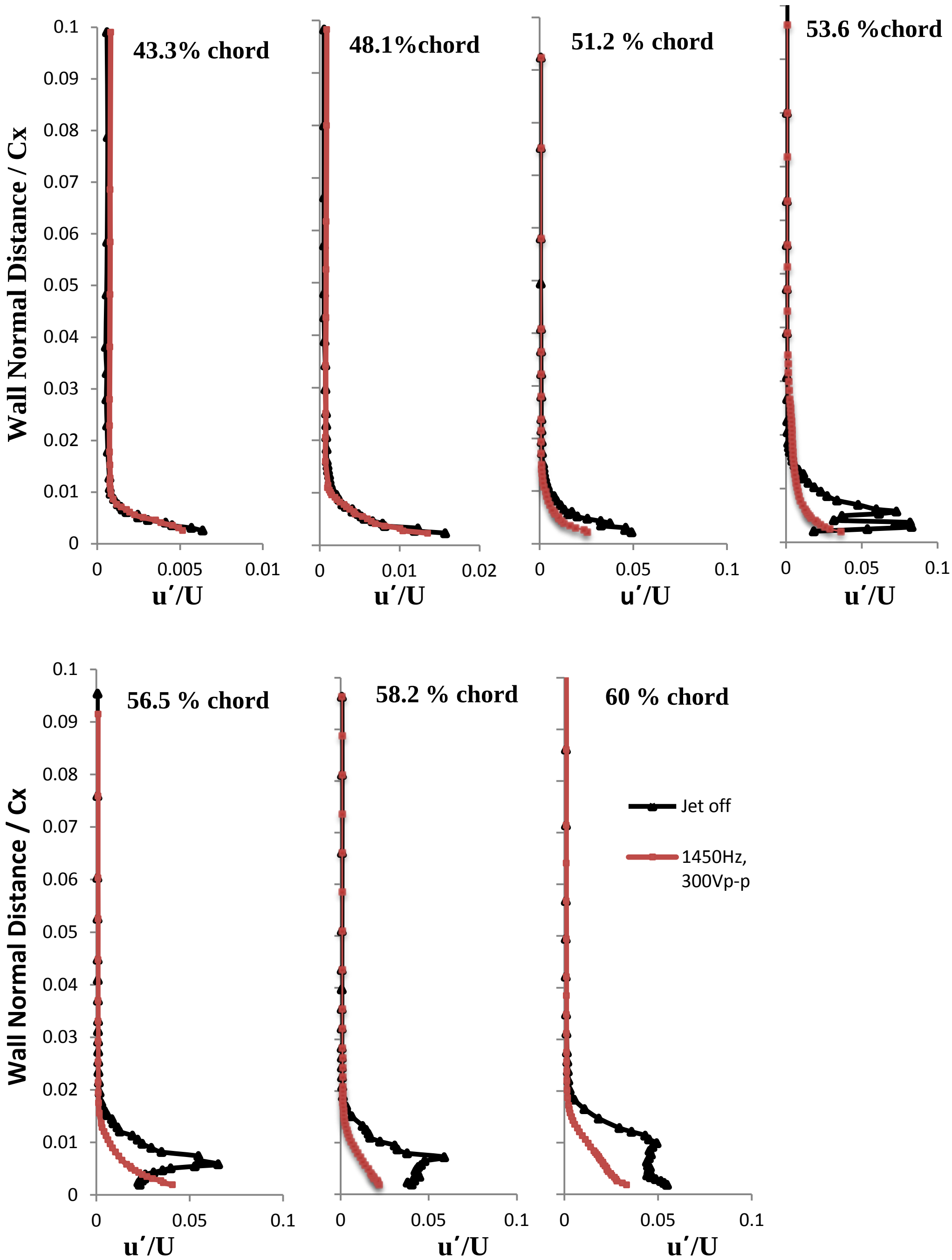

Figure 3.3.19: Turbulence intensity profiles at several chordwise locations at 2.3x10^5 Reynolds number, at zero angle of attack.

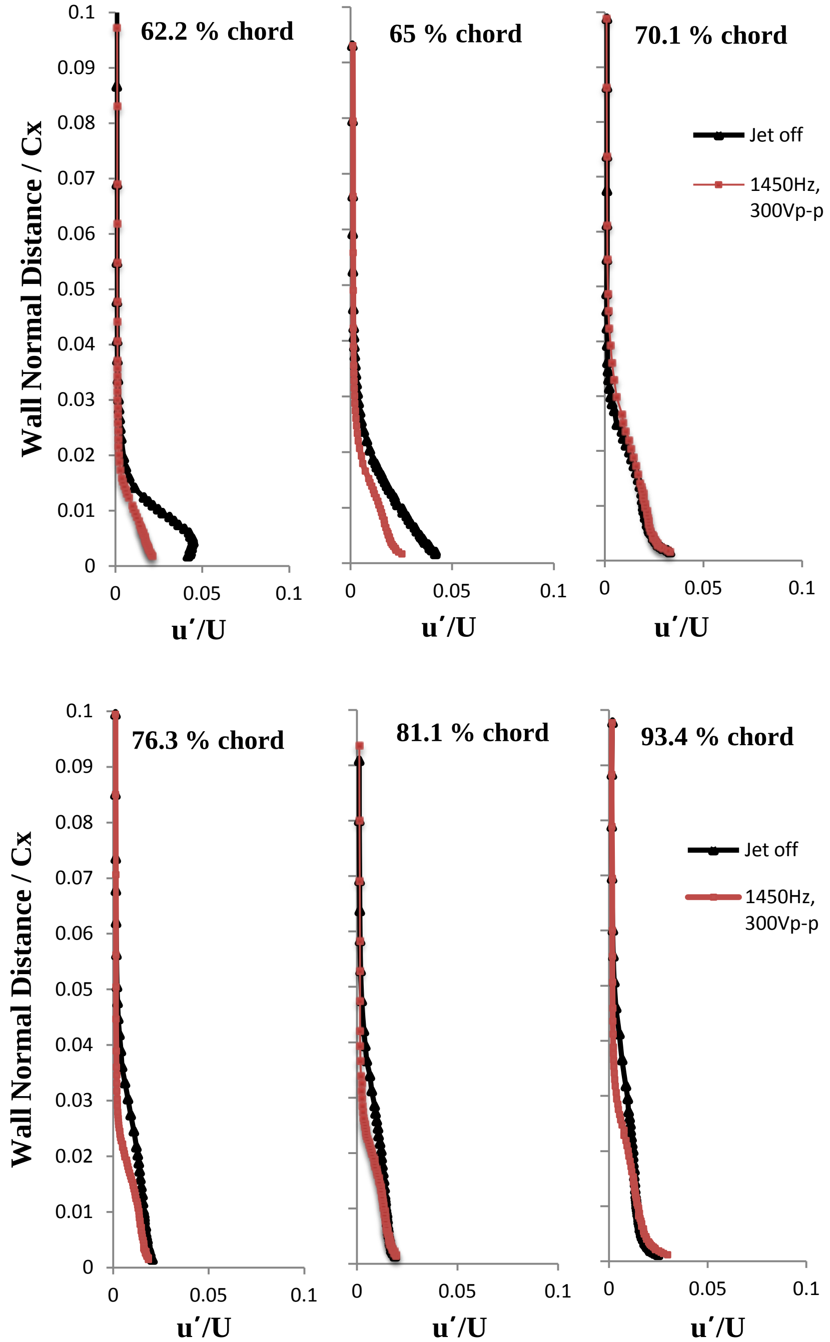

Figure 3.3.20: Turbulence intensity profiles at several chordwise locations at 2.3×10^5 Reynolds number, at zero angle of attack.

With the synthetic jet actuators on, it is observed that the clearly visible inflection points present in the mean velocity profiles of the baseline case have disappeared as seenFigure

3.3.15 and Figure 3.3.16. Also, the mean velocity profiles at each station demonstrate that the local boundary layer thicknesses have diminished in size; that is the shear layer is thinner than the baseline case. In addition, from the fluctuating velocity profiles inFigure 3.3.17 and Figure 3.3.18, it is seen that there is no peak fluctuation within the shear layer away from the wall. This also proves the absence of inflection points in the boundary layer. Furthermore, the dead air region, the strong recirculation zone, and therefore the laminar separation bubble, seem to be eliminated by the periodic excitation of the synthetic jet actuators. Furthermore, from the turbulence intensity profiles it is understood that zero mean velocities within the boundary layer also have been eliminated.

From the mean and fluctuating velocity and turbulent intensity profiles, it is obvious that the separation point as well as the transition and reattachment onsets cannot be determined with the jets on case easily. However, it is sure that the transition mode has been changed by the periodic excitation generated by synthetic jet actuators. Transition from laminar flow to turbulent flow does not occur over the laminar separation bubble anymore.

Wake Analysis

The effect of the synthetic jets on the wake profiles of the S809 airfoil at 4 mm downstream of the trailing edge is demonstrated in the following figures. Hot wire measurements were conducted at the same spanwise location with the boundary layer measurements.

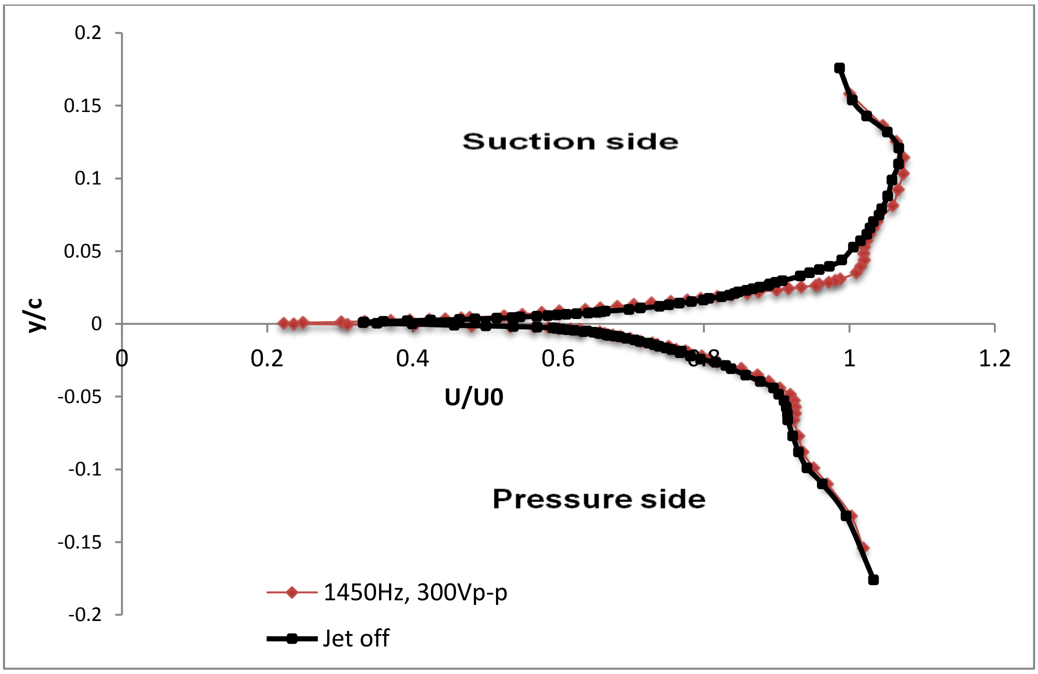

Figure 3.3.21: Mean velocity profile at 4 mm downstream the trailing edge, at $2.3x10^5$ Reynolds number and at zero angle of attack.

Figure 3.3.21shows the mean velocity profile at 4mm downstream the trailing edge of the S809 blade with and without synthetic jets. Here, the mean velocities are normalized by the mean free stream velocity, and the traversed distance along the wake thickness is normalized by the chord of the blade. From this figure it is clearly seen that at this wake location there is no effect of synthetic jet actuation on the pressure side. This is an expected result because the actuators are placed only on the suction side of the blade and since the measurement location is very close to the blade trailing edge the flow excited by the synthetic jets over the suction side cannot develop over the pressure side at the wake. Suction side, on the other hand, seems to be affected by the synthetic jets. In the figure, it is seen that the wake profile of the suction side becomes smaller. Since the flow is found to be an attached flow with a laminar separation bubble in the boundary layer at 2.3×10^5 Reynolds number and at zero angle of attack in the baseline case, the effect of the synthetic jet actuators at this wake location is not significant. However, this profile ensures that the flow is attached. Also, it can be concluded that for the detached flow conditions the effect of synthetic jets will be more significant.

Figure 3.3.22demonstrates the effect of the synthetic jets on the fluctuating velocity (turbulent fluctuations) and turbulent intensity profiles at 4mm downstream the trailing edge of the S809 blade. It is clearly seen that the same region at the suction side is affected by the synthetic jets, and the figure clearly shows that both the fluctuating velocities and turbulence intensities decrease in this region. The decrease in the fluctuating velocities and turbulence intensities is probably the cause of the decrease in the wake size in the same affected region.

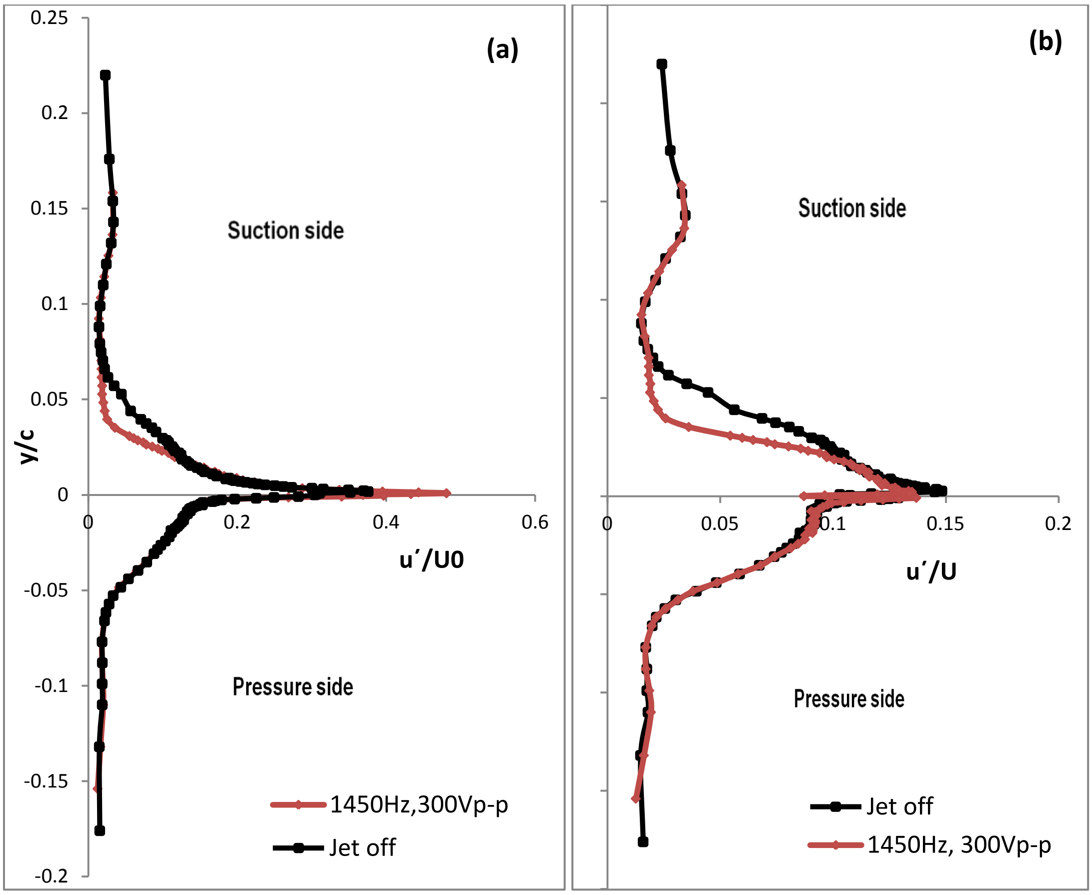

Figure 3.3.22: Wake profiles at 4 mm downstream the trailing edge of the blade at $2.3x10^5$ Reynolds number and at zero angle of attack (a) Fluctuating velocity profiles normalized by mean free stream velocity (b) Turbulence intensity profiles normalized by local mean velocity.

CHAPTER4

CONCLUSION

4.1 General Conclusions

In this thesis, the effect of synthetic jets on laminar boundary layer separation occurring on the suction side of S809 airfoil is investigated at 2.3×10^5 Reynolds number at zero angle of attack. For this purpose, first of all a 2-D blade having S809 wind turbine airfoil profile with three different configurations are designed and manufactured.

Experiments start with wind tunnel characterization with and without tested blade installed inside the tunnel in order to determine the tunnel turbulence intensities. Results of the tunnel characterization show that turbulence intensities are quite high, which may cause an early transition from laminar flow to turbulent flow. After tunnel characterization, synthetic actuator characterization is performed and an operating frequency of 1450Hz is determined to drive the actuators as a result. Then, mid span surface pressure measurements are conducted on the suction side of the airfoil in order to have a first insight about the separation problem and determine the corresponding behaviour of the pressure distribution over the surface of the airfoil. After surface pressure measurements, boundary layer measurements as well as wake measurements are performed at 2.3×10^5, 3.4×10^5 and 5.1×10^5 Reynolds numbers at zero angle of attack without synthetic jet actuators. Through the pure airfoil boundary layer measurements it is detected that a larger separation bubble occurs at 2.3×10^5,therefore, this case is decided to study the effect of the synthetic jets on the flow development. At Reynolds number of 2.3×10^5, 2D PIV measurements are also conducted to provide more information about the flow development within the separated shear layer. After mounting the array of the synthetic jet actuators at the 28% chord location over the suction surface of the blade controlled case boundary layer and wake experiments are performed at 2.3×10^5 Reynolds number at zero angle.

Results of the baseline measurements (both surface pressure measurements and boundary layer measurements) show that a laminar separation bubble occurs over the suction surface of the S809 airfoil at 2.3×10^5 Reynolds number at zero angle of attack, with a narrow wake behind the blade. Analyses of the flow behaviour within the separated boundary layer show that a dead air region and a strong recirculation region exit in the bubble. After operating synthetic jet actuators with a sinusoidal wave of 300Vp-p and 1450Hz, it is observed that the inflection points in the mean velocity profiles and peak fluctuating velocities have disappeared. As a result of the periodic excitation produced by the synthetic jet actuators, the laminar separation bubble is detected to be eliminated. In addition, the resultant mean and fluctuating velocity profiles in the wake show that jets have diminished the wake size at the suction side even for this attached flow conditions. Therefore, it can be concluded that synthetic jets can be more effective in the wake of a detached flow.

4.2 Recommendations for Further Research

Before this study there was no experimental experience and no background for an experimental study on flow control using synthetic jet actuators in the Aerospace Engineering Department. Thus, this study started with designing the experimental set up including the blade design. Now, the set up is ready and it is more easy to make contributions on this study.

Although this study has met its objectives there are some issues required to be investigated further. First of all, the effect of the synthetic jet on the flow development both within the boundary layer and at the wake should be investigated also with different angles of attacks including the post stall angles. This will help to better understand the physical process involved. Also, in order to optimize the performance of SJAs, different actuation frequency and voltage signals should be studied including the non dimensional parameters that define SJAs under cross flow. In addition, experiments should be performed at several spanwise locations in order to determine the global effect of the jets. Finally, Particle Image Velocimetry (PIV) measurements should be performed to better resolve the structure of the synthetic jet and its interaction with the adverse pressure gradient boundary layer.

REFERENCES

[1] Veers P. S. et al. (2003) Trends in the Design, Manufacture and Evaluation of Wind Turbine Blades. Wind Energy, 6.

[2] Barlas, T.K., and van Kuik, G.A.M.(2010) Review of State of the Art in Smart Rotor Control Research for Wind Turbines. Progress in Aerospace Sciences, No.46, pp 1-27.

[3] Berg, D.E., Zayas, J.R., Lobitz, D.W., van Dam, C.P., Chow, R., and Baker, J.P. (2007)Active Aerodynamic Load Control of Wind Turbine Blades. Proc. of the 5th Joint ASME/JSME Fluids Engineering Conference, San Diego, CA.

[4] Larsen T.J., Madsen H. A., Thomsen K. Active Load Reduction Using Individual Pitch Based on Local Inflow Measurements. Wind Energy No 8. pp. 67–80.

[5] Bossanyi E.A. The Design of Closed Loop Controllers for Wind Turbines. (2005) Wind Energy. 8:481–5

[6] van der Hooft EL and van Engelen TG. Feed Forward Control of Estimated Wind Speed. (2003) Technical Report, ECN-C-03-137, ECN.

[7] Hand M.M., Wright A.D., Fingersh L.J., Harris M. (2006) Advanced Wind Tturbine Controllers Attenuate Lloads When Upwind Velocity Measurements are Inputs, AIAA 2006-603. In: Proceedings of the 44th AIAA/ASME, Reno, NV, USA.

[8] Lake Barlas, T.K. (2011) Active Aerodynamic Load Control on Wind Turbines, Aeroservoelastic Modeling and Wind Tunnel Experiments. PhD thesis, Technical University of Denmark.

[9] DOE. (2005) Variable Length Wind Turbine Blade. DE-FG36-03GO13171, June 30.

[10] GE Wind Energy, LLC. (2006) Advanced Wind Turbine Program Next Generation Turbine Development Project. Subcontract Report NREL/SR-5000-38752, May.

[11] Johnson, S.J.,C.P., van Dam, C.P. and Berg, D.E. (2008) Active Load Control Techniques for Wind Turbines. Sandia Report. SDAND 4809, August.

[12] Bak, C., Gaunaa, M., Anderson, B.B., Buhl, T., Hansen, P., Clemmensen, K., and Moeller, R. (2007) Wind Tunnel Test on Wind Turbine Airfoil with Adaptive Trailing Edge Geometry. AIAA Paper 2007-1016, Jan.

[13] Hulskamp, A.W., Beukers, A., Bersee, H., van Wingerden, J.H., and Barlas, T.K. (2007) Design of a Wind Tunnel Scale Model of an Adaptive Wind Turbine Blade for Active Aerodynamic Load Control Experiments. 16th ICCM.

[14] Schlichting H. Boundary layer theory. (1979) New York: McGraw-Hill.

[15] Barrett, R., and Farokhi, S. (1996) Subsonic Aerodynamics and Performance of a Smart Vortex Generator System. Journal of Aircraft, Vol. 33, No. 2, March-April.

[16] Moreau. E. (2007) Airflow Control by Non Thermal Plasma Actuators. Journal of Phys. D, 40: 605-636.

[17] Corke, T.C., Post, M.L and Orlov, D.M.(2007)SDBD Plasma Enhanced Aerodynamics: Concepts Optimization and Applications.Progress in Aerospace Sciences 43 (2007) 193–217.

[18] Nelson, R.C., Corke, T.C.and Othman, H. (2008) A Smart Wind Turbine Blade Using Distributed Plasma Actuators for Improved Performance. Performance 46th Aerospace Sciences Meeting, January 7-10, 2008, Reno, Nevada.

[19] Stalnov, O., Kribus, A. and Seifert, A. (2010) Evaluation of active flow control applied to wind turbine blade section. J. Renewable Sustainable Energy 2, 063101

[20] Khan, Z Maldonado, V., Boucher, M., Ostman, R. and Amitay, A. (2009) Active Vibration Control of a Wind Turbine Blade Using Synthetic Jets. International Journal of Flow Control. Volume 1, Number 4 December.

[21] Jabbal, M., Zhong, S. (2008)The Near Wall Effect of Synthetic Jets in a Boundary Layer.International Journal of Heat and Fluid Flow. No 29, pp. 119–130.

[22] Smith D.R., Amitay M., Kibens K., Parekh D.E. and Glezer A. (1998) Modification of Lifting Body Aerodynamics Using Synthetic Jet Actuators; AIAA Paper 1998-0209.

[23] Hong, G. (2006) Effectiveness of Micro Synthetic Jet Actuator Enhanced by Flow Instability in Controlling Laminar Separation Caused by Adverse Pressure Gradient. Sensors and Actuators A 132 (2006) 607–615.

[24] Schaeffler, N.W. and Jenkins, L. N. (2006) Isolated Synthetic Jet in Crossflow: Experimental Protocols for a Validation Dataset. AIAA JOURNAL Vol. 44, No. 12

[25] Milanovic, I. M. and Zaman, K. B. M. Q. (2005) Synthetic Jets in Crossflow. AIAA JOURNAL Vol.43, No. 5.

[26] VGlezer, A.(1988) The formation of vortex rings; Phys. Fluids, Vol.31, No. 12, pp. 3532-3542, Dec.

[27] Jabbal, M., Zhong, S. (2008)The near Wall Effect of Synthetic Jets in a Boundary Layer. International Journal of Heat and Fluid Flow 29 (2008) 119–130

[28] Carmichael, B. H. (1981) Low Reynolds Number Airfoil Survey. NASA CR 165803, Vol. I.

[29] Mueller, T. J & DeLaurier, J. D. (2003) Aerodynamics of Small Vehicles. Annual Reiew of Fluid Mechanics. 35, 89–111.

[30] Zhang, X. F. (2005) Separation and Transition Control on Ultra-High-Lift Low Pressure Turbine Blades in Unsteady Flow. PhD Thesis. Cambridge University.

[31] Tani, I. (1964) Low Speed Flows Involving Bubble Separations. Prog. Aerosp. Sci. 5, 70–103.

[32] O'Meara, M. M., and Mueller, T. J. (1987) Laminar Separation Bubble Characteristics on an Airfoil at low Reynolds Numbers. AIAA Journal, Vol. 25, No. 8, pp. 1033-1041.

[33] Mayle, R.E. (1991) The Role of Laminar-Turbulent Transition in Gas Turbine Engine. ASME Journal of Turbomachinery, 113, pp. 509-537

[34] A. Pope and J.J. Harper, Low Speed Wind Tunnel Testing, Wiley, New York 1966.

[35] Face Inc. Retrieved from http://www.prestostore.com/cgibin/pro23.pl?ref=thunderonline&ct=36234

[36] Ugrina, S. (2007) Experimental Analysis and Analytical Modeling of Synthetic Jet-Cross Flow Interactions. PhD Thesis.University of Maryland

[37] Shaw, R. (1959). The Influence of Hole Dimensions on Static Pressure Measurements. University of Liverpool.

[38] McKeon, B.J. and Smits, A.J.(2002) Static Pressure Correction In High Reynolds Number Fully Developed Turbulent Pipe Flow.Institute Of Physics Publishing. Meas. Sci. Technol. 13 (2002) 1608–1614

[39] Bruun H H 1995 Hot-wire Anemometry (Oxford: Oxford University Press)

[40] Gallas, Q. (2005) On The Modeling And Design Of Zero-Net Mass Flux Actuators. PhD Thesis. University Of Florida.

[41] Burgmann, S. And Schröder, W. (2008) Investigation Of The Vortex Induced Unsteadiness Of A Separation Vbubble Via Time-Resolved And Scanning PIV Measurements. Exp Fluids (2008) 45:675–691

[42] McAuliffe, B. (2003). An Experimental Study of Flow Control Using Blowing For a Low-Pressure Turbine Airfoil. MSc Thesis. Carleton University.

[43] A. Hatman, T. Wang. (1998) A Prediction Model for Separated-flow Transition, ASME Paper GT-98-237, ASME Turbo Expo ’98, Stockholm, Sweden.

[44] Uzol, O., Brzozowski, D., Chow, Y. C., Katz, J., Meneveau, C. (2007). A Database of PIV Measurements within a Turbomachinery Stage and Sample Comparisons with Unsteady RANS. Journal of Turbulence, Vol. 8.